

# Discontinuous Long Fibre Reinforced Thermoplastic for Additive Manufacturing

S.H. Han

Delft University of Technology



# Discontinuous Long Fibre Reinforced Thermoplastic for Additive Manufacturing

by

S.H. Han

to obtain the degree of  
Master of Science Aerospace Engineering  
at the Delft University of Technology

Thesis committee:	Dr. K. Masania	TU Delft	Chair, daily supervisor
	ir. C. van Wingerden	CEAD	Company supervisor
	Dr. O.K. Bergsma	TU Delft	Examiner
	ir. J. Sinke	TU Delft	Examiner

Publicly defended: 3rd October 2022 13:00  
at the Faculty of Aerospace Engineering, Delft



# Abstract

Current large-scale additive manufacturing extruders use short reinforcing fibre-filled thermoplastic pellets, which marginally improve the mechanical performance but are too short to exploit the strength of the fibres fully. Long fibre pellets have much higher potential strength, and the development of higher strength materials could create stronger parts and/or reduce the mass of products, lowering their energy consumption in the case of vehicular parts of heated tooling.

By developing long-fibre thermoplastic pellet processing, this thesis works toward improving the mechanical performance of fused granulate fabricated parts. Extreme die-swell was encountered when extruding long glass-fibre polypropylene pellets. This die-swell is theorised to be caused by energy storage in an entangled network of long fibres, which is released upon extrusion. This issue was solved by developing a mix of two different material pellets, which was used with the tactical use of temperature zones to create a hetero-phasic blend inside the extruder. This technique and material blend enable controlling the melting of the long fibre pellet resin, lubricating the pellets to promote macro-alignment, and reducing heating through shear friction. These effects delay the dispersion and entangling of fibres.

This method eliminated the problem encountered; reducing porosity by 82%, increasing strength by 960% over the original swollen material and achieving specific strength 16% higher than the short fibre compound currently being used. This research presents a new method to make previously un-processable long fibre thermoplastic pellets useable with a 25 mm diameter screw extruder. It contributes to the development of unprecedented high-performance parts 3D printed at a large scale.



# Acknowledgements

I want to take this opportunity to acknowledge everyone who has helped me throughout this thesis. I had the good fortune of having the support of two wonderful teams during this project.

Firstly, I would like to thank the Shaping Matter Lab and especially my supervisor Dr Kunal Masania, who provided constant support and has formed an amazing group of students and researchers. It has been wonderful and a lot of fun working with so many brilliant scientists and 3D printing enthusiasts!

Doing my thesis at CEAD has made this past year very interesting. I had the opportunity to see and experience the brilliance, chaos and sometimes insanity that goes into engineering and applying their large-scale 3D printing hardware. I would like to thank my company supervisors, Charléne van Wingerden, Lucas Janssen, Robert Thompson and Mark Muilwijk, who always made time for me and had lots of suggestions, but also gave me the freedom to explore. I wish the company continued success and hope this work will be useful.

Finally, a thank you to my friends and family who supported and put up with me over the last year. It has been a challenging year, and though I regret not achieving everything I had hoped, I am proud of the result. I hope that you, the reader, enjoy reading this thesis.

Master of Science and *ingenieur*,  
S.H. Han  
Delft, October 2022



# Contents

<b>Acknowledgements</b>	<b>ii</b>
<b>1 Introduction</b>	<b>1</b>
1.1 Fibre Reinforcement . . . . .	3
<b>2 State-of-the-Art</b>	<b>5</b>
2.1 Short-Fibre Reinforced AM . . . . .	5
2.1.1 Fused Filament Fabrication . . . . .	5
2.1.2 Fused Granulate Fabrication . . . . .	6
2.2 Continuous Fibre Composite AM . . . . .	7
2.2.1 Over-wrapping with tape . . . . .	9
2.3 Existing use of long-fibre compounds . . . . .	10
2.3.1 Long-fibre extrusion for additive manufacturing . . . . .	11
2.4 Thesis Definition . . . . .	12
<b>3 Experimental Setup</b>	<b>13</b>
3.1 Screw Extruder . . . . .	13
3.1.1 Material used . . . . .	14
3.2 Extrusion Analysis . . . . .	14
3.3 Mechanical Testing . . . . .	18
<b>4 Initial Investigation</b>	<b>21</b>
4.1 Conventional Polymer Die-swell . . . . .	21
4.2 Fibre/Nozzle Interaction . . . . .	22
4.2.1 Fibre entanglement . . . . .	25
4.3 Ineffectiveness of Traditional Fibre Alignment . . . . .	26
4.4 Reducing Residence Time . . . . .	28
<b>5 Hetero-phasic Pellets for Pre-alignment and Lubrication</b>	<b>31</b>
5.1 PP/PE blend . . . . .	31
5.1.1 Printability . . . . .	32
5.2 Working Mechanism . . . . .	34
5.3 Mechanical Performance . . . . .	38
5.4 Microstructure Characterisation . . . . .	39
5.4.1 Fibre length . . . . .	39
5.4.2 Fibre orientation . . . . .	40
5.4.3 Summary of measured fibre efficiency factors . . . . .	41
<b>6 Conclusions &amp; Recommendations</b>	<b>43</b>
6.1 Recommendations . . . . .	44
<b>References</b>	<b>46</b>

# List of Tables and Figures

1.1	Comparison of the scale of desktop and large-scale AM machines . . . .	1
1.2	Survey results from ‘State of 3D Printing 2021’ which highlights the strength and low-cost as the two highest material selection criteria . . . .	2
1.3	Schematic diagram of shear lag model showing load transfer from matrix to fibre in a composite . . . . .	3
1.4	Fibre orientation factor efficiency as a function of misalignment angle . . .	4
1.5	Tensile strength vs fibre length of discontinuous aligned 30% W/W glass-fibre polypropylene . . . . .	4
2.1	Cross-section of desktop Fused Filament Fabrication print showing short carbon fibre reinforcements . . . . .	5
2.2	Liquid Crystal Polymer printing, showing the hierarchical shear alignment of nematic crystal domains . . . . .	6
2.3	Large-scale Fused Granulate Fabrication 18 mm bead extrusion . . . . .	7
2.4	Large-scale AM box print that has collapsed due to overheating . . . . .	7
2.5	Markforged 3D printed part with white nylon, reinforced by continuous black carbon fibre reinforcement . . . . .	8
2.6	9T Labs post-consolidation process, which joins separately printed parts together . . . . .	8
2.7	Continuous Fibre AM extruder . . . . .	9
2.8	Scalable Composite Robotic Additive Manufacturing system . . . . .	9
2.9	Illustration of fibre fillers in long vs short fibre pellet . . . . .	10
2.10	Long fibre pellet manufacturing by pultrusion process . . . . .	10
2.11	Overview comparison of long vs short fibre compound . . . . .	11
2.12	12 mm fibre pellet extrusion test . . . . .	12
3.1	Anatomy of a screw extruder . . . . .	13
3.2	Fibre content, lengths and resins in pellets used . . . . .	14
3.3	11 mm LGFPP pellets, 1 euro coin for scale . . . . .	14
3.4	Calcination of printed samples, long fibre pellets and short fibre pellets .	15
3.5	ImageJ automatic fibre length detection . . . . .	16
3.6	ImageJ automatic fibre orientation measurement . . . . .	17
3.7	Method of Ellipses, estimating fibre angle by measuring cross-sectional ellipticity . . . . .	17
3.8	Cross-section of a curved fibre . . . . .	17
3.9	Deformation of extruded material when sheared against the previous layer . . . . .	18
3.10	Three-point bending mechanical test setup, 10 mm diameter end supports 120 mm apart, 20 mm diameter indenter . . . . .	19
4.1	Die swell due to polymer elasticity . . . . .	21

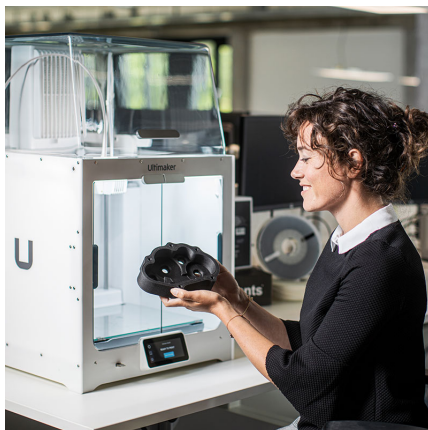
4.2	Sectioned microscopy of original long fibre extrusion . . . . .	22
4.3	Extrudate swelling vs nozzle temperature setting . . . . .	22
4.4	Extruded long glass fibre polypropylene material showing swelling behaviour . . . . .	23
4.5	Extrudate swelling vs input fibre length . . . . .	24
4.6	Extrudate swelling vs nozzle diameter . . . . .	24
4.7	Injection moulded long fibre thermoplastic part . . . . .	25
4.8	micro CT slices of LGFPP40% fibre loading exposed to a shear flow for different residence times . . . . .	25
4.9	Fibre-fibre interaction regions according to density and fibre length . . .	26
4.10	Extrudate swelling vs screw RPM . . . . .	26
4.11	Simplified parabolic shear flow fibre alignment . . . . .	27
4.12	Types of fibre motion in a Couette velocity flow field . . . . .	28
4.13	The four individually temperature controllable zones of the CEAD E-25 extruder . . . . .	28
4.14	Extrudate swelling vs transport temperature setting . . . . .	29
4.15	Fibre morphology of long GF PP collected from screw pull-out . . . . .	29
5.1	Mixed pellet input, black long glass fibre polypropylene pellets with lower temperature melting white HDPE for lubrication . . . . .	31
5.2	Extrudate swelling vs additive content . . . . .	32
5.3	The dramatic effect of HDPE on swelling reduction . . . . .	33
5.4	Printed layers with 15% modified LGFPP . . . . .	34
5.5	Shear viscosity at 1/s shear rate of HDPE and PP . . . . .	35
5.6	Melting peaks characterised by DSC of PP, HDPE and their blends . . .	35
5.7	Hetero-phasic pellet transition along the screw extruder . . . . .	36
5.8	Effect of wall slip on the shear flow field . . . . .	37
5.9	Interface between two polymers of different viscosity causes a region of lower viscosity . . . . .	37
5.10	Sectioned microscopy of LGFPP/PE blend, showing a white region of discrete unmixed HDPE inside darker PP . . . . .	37
5.11	Sectioned microscopy of LGFPP/PE blend, showing un-dispersed fibre agglomerates . . . . .	37
5.12	Stress-strain curves from three-point bending . . . . .	38
5.13	Average porosity . . . . .	38
5.14	Average specific flexural strength . . . . .	38
5.15	Average specific flexural stiffness . . . . .	38
5.16	Sample fibre content, average density, sample count used for mechanical testing . . . . .	39
5.17	Average strength, stiffness, calculated specific strength and stiffness values from mechanical testing . . . . .	39
5.18	Fibre length efficiency factor . . . . .	39
5.19	Fibre length distribution histograms . . . . .	40
5.20	Fibre orientation efficiency factor . . . . .	40
5.21	Fibre orientation distribution histograms . . . . .	41
5.22	Sectioned microscopy showing large central pore . . . . .	42
5.23	Fibre efficacy terms and specific strength for reference . . . . .	42



## Introduction

Additive manufacturing (AM), also known as 3D printing, is a family of digital manufacturing techniques. A part is created from 3D CAD data by the successive addition of materials, often in a layer-by-layer process [1]. Some benefits of AM are very low material waste (with buy-to-fly ratios of near 1:1 [2]), high design-freedom and near-zero set-up time [3] and product-specific tooling; these characteristics allow the creation of parts almost directly from CAD geometry.

However, the technique is not without its flaws. Being typically restricted to small part sizes, slow manufacturing speed, high costs per part, and lower mechanical properties compared to more traditional processes have largely limited AM to prototyping and other low-series production work. For AM to expand in the end-use product market, considerable improvements must be made in these aspects to make them competitive and viable alternatives to traditional methods.



(a) Ultimaker desktop 3D printer



(b) CEAD Large-scale Additive Manufacturing printer<sup>1</sup>

**Figure 1.1:** Comparison of the scale of desktop and large-scale AM machines

In contrast to desktop-sized machines (example pictured in Figure 1.1a), which produce parts typically smaller than 20 cm in any dimension, Large Scale Additive Manu-

<sup>1</sup><http://www.ceadgroup.com>

facturing (LSAM, example pictured in Figure 1.1b) refers to prints of an order of magnitude higher, with typical part sizes of 1 m or more. By mounting a high flow-rate extruder on a large motion platform, larger prints can be produced in less time, addressing AM's low manufacturing speed at the cost of rougher detail resolution and surface finish.

LSAM is used to produce some end-use parts of larger products such as vehicles, furniture or buildings. Especially uses-cases with low production numbers, custom bespoke products or prototyping where the advantages above make AM the most suitable manufacturing method is where LSAM excels. Moulds for composite production or metal sheet forming are also interesting use cases for LSAM. Composite AM moulds can compete with expensive invar steel tooling in closely matching carbon fibre's low coefficient of thermal expansion. Near-net-shape 3D printed moulds can be milled to a suitable surface finish in a fraction of the time it would take to machine the same mould from a block of material.

One aspect in which AM-produced products fall behind traditional manufacturing is the material's mechanical properties. While thermoplastics are suitable for extrusion-based AM due to their relatively lower energy requirements and melt viscosity than metals, but they also tend to have lower mechanical properties. This limits 3D printed parts to use cases with low loading requirements, or parts must be made with oversized wall thicknesses to compensate for their low strength. Figure 1.2 shows that material strength is the highest driver for material selection among polled AM users. Better AM materials are required to become more competitive against traditional manufacturing processes.

Q: What are your top 3 requirements for material selection?

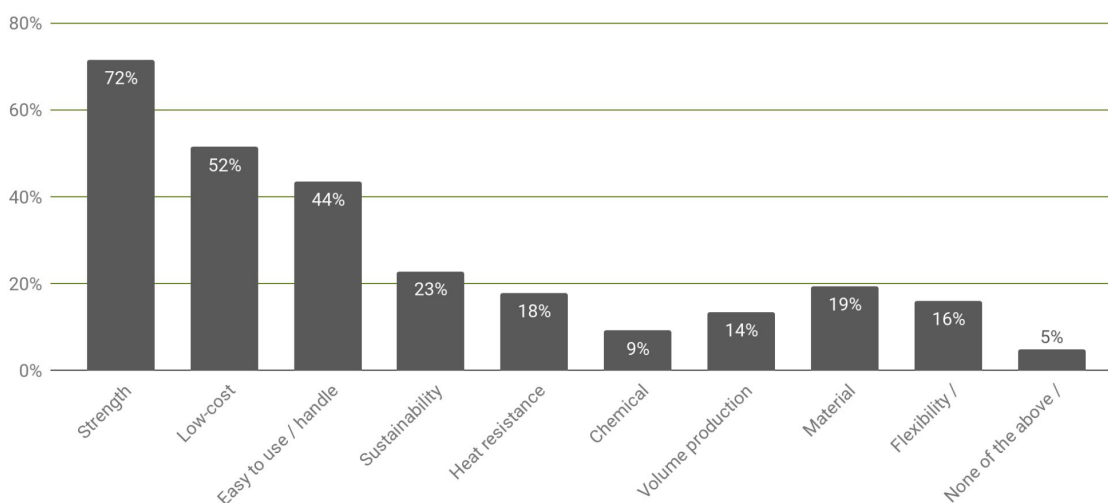


**Figure 1.2:** Survey results from 'State of 3D Printing 2021' which highlights the strength and low-cost as the two highest material selection criteria [4]

Especially weight-specific properties are crucial for producing parts with less mass of the same mechanical requirements. Lower part mass corresponds to a lower environmental impact from manufacturing the part and also lowers the cost and environmental footprint during the product's lifetime. For moving vehicles or parts that need to

be transported, lower mass equates to lower energy use and emissions. For heated tools such as autoclaved composite moulds, lower mass requires less energy to bring up to process temperatures. This is significant as combating global warming through lowered energy use, and CO<sub>2</sub> emissions is a crucial challenge that must be met for the future sustainability of the Earth.

## 1.1. Fibre Reinforcement

To enhance the mechanical properties of 3D printed material, fibre fillers can be introduced to reinforce the resin. A composite material with improved properties is formed by embedding fibres stiffer and stronger than pure resin [5, 6]. These fibres can be discontinuous or continuous in length and typically made of glass fibre (GF) or carbon fibre (CF). Discontinuous fibre compounds are further differentiated as short or long fibre compounds (with 1 mm typically being the boundary length between short and long).

When a composite material is loaded and strained, the stiffer fibre takes up most of the load. The resin matrix transfers these loads to the fibre by shear stresses along the sides of the fibre, which is taken up by axial stress in the fibre. The strength of a composite is affected by the strength of the fibre  $\sigma_f$ , the strength of the matrix  $\sigma_m$  and the ratio of fibres, the fibre volume fraction  $V_f$  as shown in Equation 1.1. This Kelly-Tyson [7] form of the rule-of-mixtures equation also has two additional parameters, the orientation efficiency  $\eta_0$  (Equation 1.2) and the fibre loading efficiency  $\eta_l$  (Equation 1.3), to account for fibre orientation and fibre length, respectively.

$$\sigma = \eta_0 \eta_l V_f \sigma_f + (1 - V_f) \sigma_m \quad (1.1) \quad \eta_0 = \sum_n a_n \cos^4(\phi_n) \quad (1.2)$$

$$\eta_l = \begin{cases} (1 - \frac{l_c}{2l}), & l \geq l_c \\ \frac{l}{2l_c}, & l < l_c. \end{cases} \quad (1.3) \quad l_c = \frac{D \sigma_f}{2\tau} \quad (1.4)$$

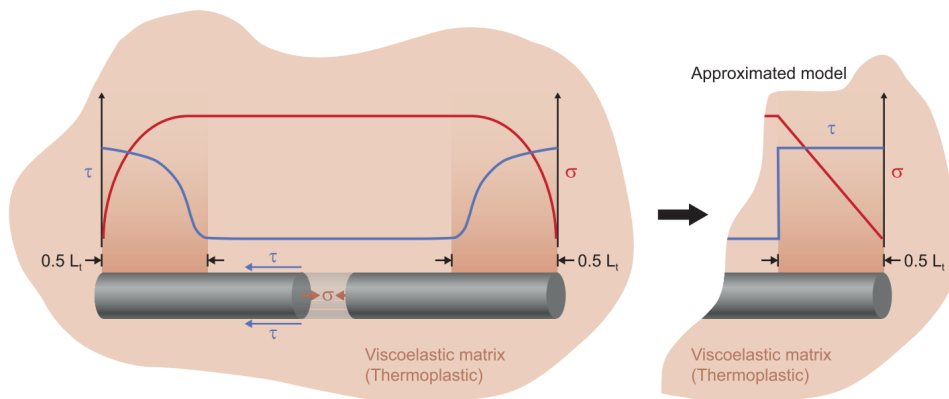


**Figure 1.3:** Schematic diagram of shear lag model showing load transfer from matrix to fibre in a composite, where  $\tau$  is the interfacial shear stress, and  $\sigma_f$  is the axial fibre stress,  $D$  is the fibre diameter and  $L_t$  is the load transfer length [6]

As the fibres mostly carry load axially, the orientation and alignment of the fibres with the load direction are critical for anisotropic properties. The efficacy of the fibre can be quantified by orientation efficiency factor  $\eta_0$  with Equation 1.2, which is a fibre fraction

( $a_n$ ) weighted average of the fourth power cosine of the angle between stress and fibre direction. Equation 1.2 is shown graphically in Figure 1.4.  $\eta_0$  is equal to 1 for perfectly aligned fibres, 0 for perfectly perpendicularly aligned fibres and 0.375 for randomly distributed fibres [8].

The fibre length efficiency factor  $\eta_l$  is related to the length of the fibre relative to the 'critical fibre length'. The critical fibre length  $l_c$  is dependent on the fibre strength, interfacial shear strength of the bond between the fibre and matrix and the diameter of the fibre, and the simplified form (approximating the shear stress as constant over the length) is illustrated in Figure 1.3 and given in Equation 1.4. Fibres longer than the critical fibre length can be fully loaded until the fibre is broken, achieving maximum strength out of the fibre. However, fibres shorter than the critical fibre length fail at the interfacial bond as shear stresses rise beyond their strength as loads are spread over the insufficient interfacial surface area.

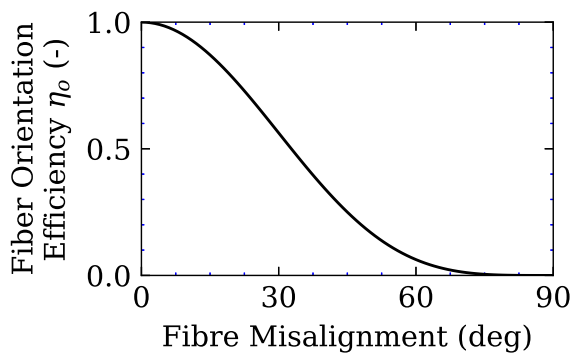


**Figure 1.4:** Fibre orientation factor efficiency as a function of misalignment angle

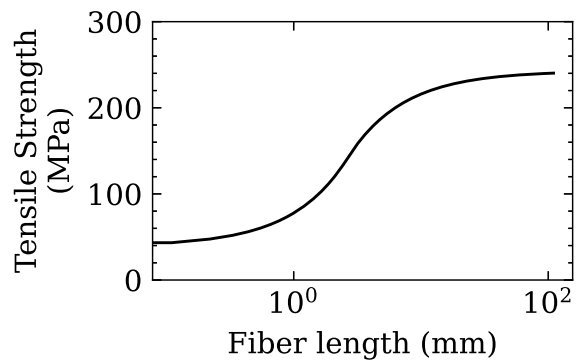


**Figure 1.5:** Tensile strength vs fibre length of discontinuous aligned 30% W/W glass-fibre polypropylene, tensile strength of the composite increases with fibre length before plateauing at the critical fibre length

Composite strength is illustrated in Figure 1.5 for 30% W/W glass fibre polypropylene which Thomason [9] has experimentally validated. It shows a significant increase in strength from increasing fibre length, as longer fibres require more force to cause fibre pull-out, before diminishing returns past the critical fibre length, as fibres get long enough to cause fibre rupture. Currently, short-fibres much shorter than the critical fibre length are being used. This steep increase in strength caused by increasing fibre length toward this critical length is a promising way of increasing material strength.

# 2

## State-of-the-Art

This chapter will give an overview of the state of the art of 3D printing with reinforcing fibres, with a scope limited to extrusion-based AM technologies. It will discuss the advantages and limitations, especially for scaling up to LSAM. Also, the use of Long Fibre Thermoplastic (LFT) pellets in other industries will be discussed. Finally, the chapter concludes with gaps identified in the technology and research and states the thesis research question.

### 2.1. Short-Fibre Reinforced AM

#### 2.1.1. Fused Filament Fabrication

Patented in 1989, Fused Deposition Modelling (FDM) [10] was a novel technique for extruding liquefied thermoplastic filament to build up a three-dimensional part in a layer-by-layer fashion. With the expiry of the FDM patent in 2009, an open-source version was developed under the new moniker Fused Filament Fabrication (FFF). Affordable machines appeared and the desktop-sized 3D printing market grew in popularity.

Zhong et al. [12] introduced carbon fibre reinforcements to ABS resin to create the first fibre-reinforced FDM parts. Similar filaments are now offered with a wide variety of resins and fibres which can be used with virtually all FDM/FFF printers. The only requirement is a hardened nozzle to avoid abrasion from the hard fibres.

The high degree of fibre alignment is achieved (pictured in Figure 2.1) as shear flow gradients inside the nozzle align with the flow direction, but the fibre fraction (10~15% W/W) and fibre lengths (~200  $\mu\text{m}$ ) are low to avoid nozzle clogging,

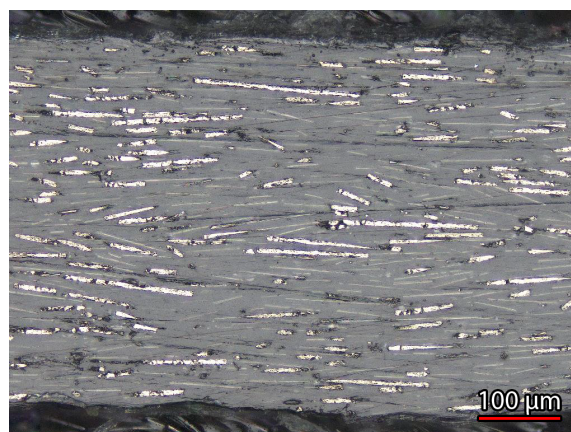


**Figure 2.1:** Cross-section of desktop Fused Filament Fabrication print showing short carbon fibre reinforcements [11]

which limits the increase in mechanical performance [13, 14]. An additional benefit from fibre fillers is in lowering the CTE, which significantly benefits the warping/shrinkage defects of prints.

A promising alternative to fibre-filled FFF is the use of Liquid Crystal Polymer (LCP). Gantenbein et al. [15] used Vectra, aligning crystal domains (instead of fibres) with the flow direction by shear alignment (as illustrated in Figure 2.2), achieving very high anisotropic properties with a shell-core architecture (with aligned crystal domains in the shell), while avoiding the previously mentioned nozzle clogging issue due to the absence of fibres. However, due to the shell-core architecture, properties are improved best with very thin layer heights and widths, which makes the technology not readily scalable for LSAM.

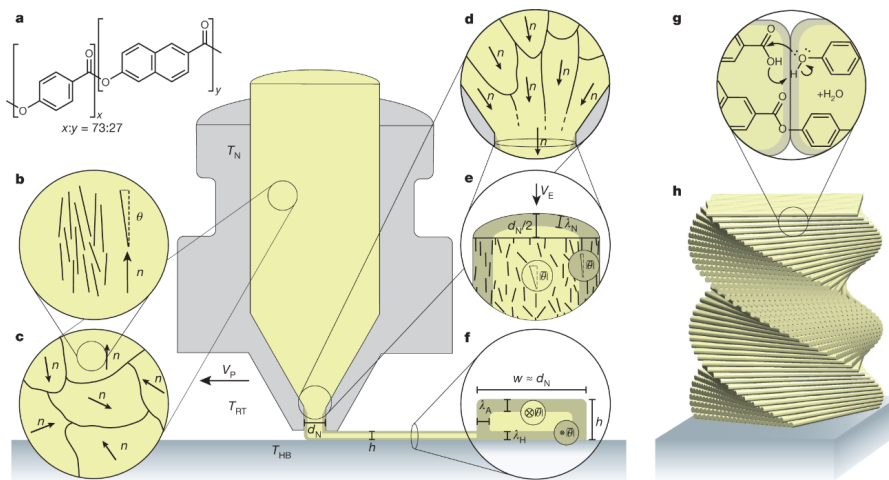


**Figure 2.2:** Liquid Crystal Polymer printing, showing the hierarchical shear alignment of nematic crystal domains for anisotropically improved properties. Alignment of crystal domains and, therefore properties are highest in the shell of the core-shell architecture of extrudates. This causes properties to decrease with [15]

FFF, in general, is also not suitable for scaling up; print speed is limited by the ability to liquefy filament quickly enough to be extruded. Heat must conduct through the nozzle walls inward until the filament's entire thickness is liquefied before reaching the nozzle orifice. This liquefaction time depends on the filament's thickness, the nozzle walls' temperature and the filament material's thermal conductivity. As mass/volume flow rate increases, the surface area of the nozzle walls used for heating does not scale linearly with the flow rate due to the square-cube rule, which limits the liquefaction and, therefore extrusion rate.

### 2.1.2. Fused Granulate Fabrication

Like FFF, Fused Granulate Fabrication (FGF) extrudes liquefied thermoplastic resin (Figure 2.3). However, instead of producing filament from resin pellets (granulate) to be used as feedstock, a screw extruder is used to use pellets as feedstock directly. While this increases the complexity, size and cost of the extruder, it allows for a much higher material flow rate and skipping the intermediary step of producing filament reduces material cost by an order of magnitude.

By mounting an FGF screw extruder to an industrial robot arm, as shown in Figure 1.1b

or to a large gantry robot, the combination of a large build volume and high printing speed enables LSAM. A wide array of materials are available for use with FGF screw extruders. Fibre-reinforced pellets are used as a standard to combat the large warping forces resulting from producing large prints [16]. The fibre lengths are similar to those used in FFF ( $\sim 200\ \mu\text{m}$ ) but with a higher fibre fraction (30% W/W being standard) as nozzle clogging is not an issue with nozzles 10~20x large in diameter than FFF.

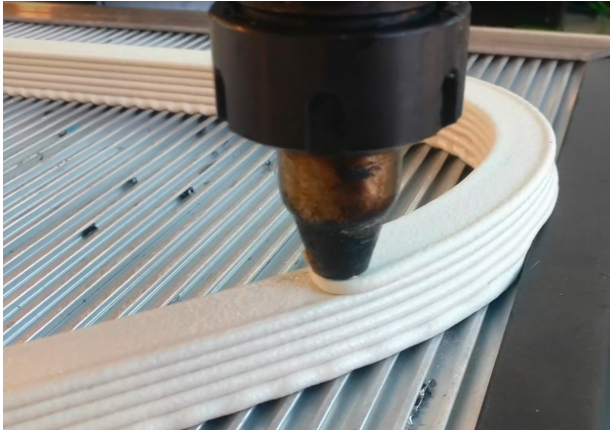


**Figure 2.3:** Large-scale Fused Granulate Fabrication 18 mm bead extrusion



**Figure 2.4:** Large-scale AM box print that has collapsed due to overheating from printing too fast [17]

While material flow rate is not typically the limiting factor, LSAM FGF also has limits based on the rate of thermal cooling. Printing speed must be fast enough to lay down successive layers of material while the substrate is still hot enough to ensure good interlayer bonding. This is an issue for high-temperature compounds such as PAEK polymers, where maintaining a high enough temperature can be challenging. The ability to print large (in terms of toolpath distance per layer) parts with high-temperature materials are limited by the motion platform's velocity and extruder flowrate capability to keep up with the printing speed requirement.

However, if the printing speed is too high for low-temperature resins, previous layers don't have enough time to cool before more material and heat are added [18, 16]. If heat buildup gets excessive, the material gets too soft to support itself and sagging or wall collapse can occur as shown in Figure 2.4. Applying LFT to LSAM could be beneficial for printing speed as they have improved stiffness past the glass-transition temperature of the resin, allowing prints to print faster without the risk of thermal collapse.

## 2.2. Continuous Fibre Composite AM

Continuous fibre printing is already commercially available on the market, with Markforged<sup>1</sup> releasing the first product. These printers combine FFF extrusion of resin to build up the part geometry and lay down continuous fibre reinforcements in critical areas. Toolpath placement and direction determine fibre placement and direction. While

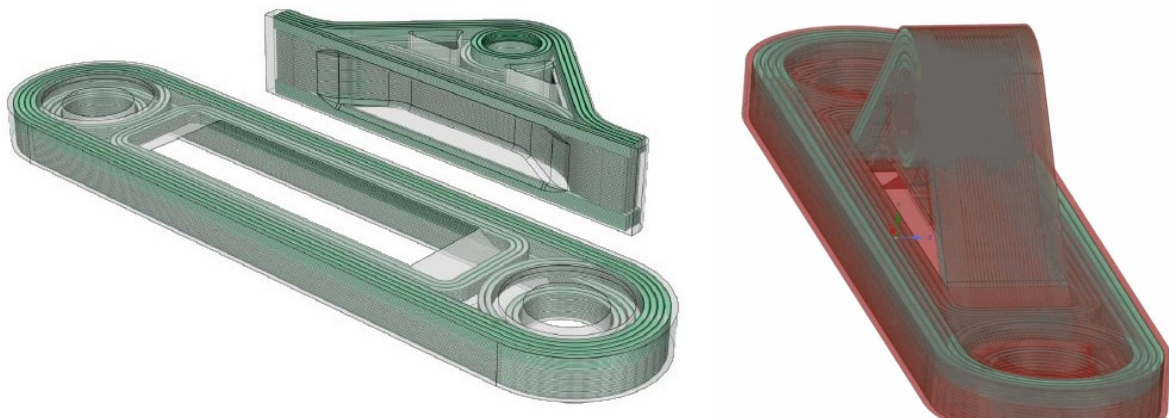
<sup>1</sup><https://markforged.com/>

significantly improving mechanical properties in the XY plane of the part (due to their Cartesian gantry printer being limited to laying down the fibre in the XY plane), this planar fibre placement limits the ability to print parts with reinforcements for multiple/out-of-plane loads directions.

To tackle this problem, 9T Labs<sup>2</sup> creates parts in multiple stages (Figure 2.6a) and then joins them together in their *Fusion Module*, which uses a heated mould press to post-consolidate parts together. This achieves a part with fibres in multiple planes (shown in Figure 2.6b) at the cost of having to create part-specific moulds for every new product. Unfortunately, this negates one of the main advantages of AM, increasing the setup cost for a new part and making large-scale prints cost-prohibitive as large moulds and presses would be required to encapsulate large prints and apply enough pressure for post-consolidation.



**Figure 2.5:** Markforged 3D printed part with white nylon, reinforced by continuous black carbon fibre reinforcement



**(a)** Parts printed separately with continuous fibre reinforcement shown in green

**(b)** Part after post-consolidation, this allows fibres to be placed in two different planes to better align fibres with three-dimensional loading cases

**Figure 2.6:** 9T Labs post-consolidation process, which joins separately printed parts together

Co-extrusion of filament also has challenges when being scaled up for LSAM. CEAD has also developed a large-scale extruder with fibre co-extrusion. The *Continuous Fibre AM (CFAM)* extruder extrudes pre-impregnated continuous CF filament together with screw extruded resin melt as shown in Figure 2.7. However, similar to the issues

<sup>2</sup><https://www.9tlabs.com/>

with scaling up FFF, trying to melt a filament with surface area-based heating limits the speed at which the filament can be heated. This resulted in fibre content of less than 10% W/W, as not enough fibre could be extruded quickly enough to keep up with the requirements of LSAM; this limits the mechanical benefit from the fibres. The low fibre content is also placed at the centre of printed beads, placing the stiff fibre near the neutral line, offering minimal benefit to the bending stiffness of single bead walls.

Another issue encountered was that fibres tended to shift toward the inner radius of curved paths as the extruder head pulled them. This is an issue with LSAM as larger printed beads contain more heat and cool down and solidify more slowly due to the cube-square law. When the resin is soft and too much tension is applied to the fibre by the tool head, defects can be created by fibre tows being pulled out of the inner radii of printed paths.

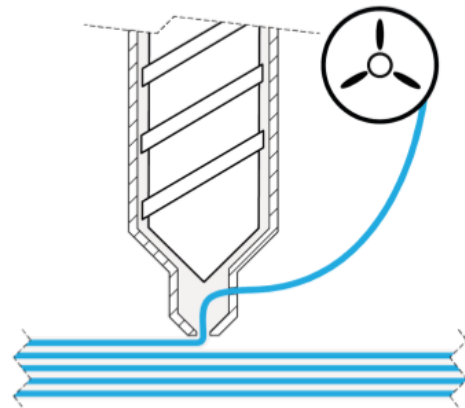
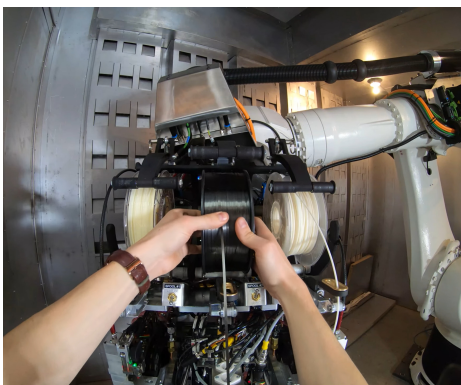


**Figure 2.7:** Continuous Fibre AM extruder, continuous filament (shown in blue) is co-extruded with thermoplastic resin being extruded by a screw extruder

### 2.2.1. Over-wrapping with tape

Another solution to create fully three-dimensional parts is to use a multi-axis system. Electroimpact<sup>3</sup> uses a dual-head, first printing a scaffold geometry with FFF, then wrapping the part with Automated Fibre Placement (AFP) for reinforcements; this allows for complex shapes to be reinforced with fibres. While using AFP reinforcement allows for a lightweight but very strong reinforcement shell, the need to create a FFF scaffold increases weight and material cost. The FFF extruder is limited by a slow material flow rate and the application of AFP reinforcement costs more time as it is done in a separate step.



(a) SCRAM print-head combining plastic extruder with and fibre tow placement head



(b) SCRAM fibre over-wrapping on top of 3D printed scaffold

**Figure 2.8:** Electroimpact's Scalable Composite Robotic Additive Manufacturing (SCRAM) system, which combines a 3D printing extruder with an automated fibre placement tool for over-wrapping reinforcements

<sup>3</sup><https://www.electroimpact.com/>

## 2.3. Existing use of long-fibre compounds

Long Fibre Thermoplastics (LFT) has grown in popularity in injection moulding in recent years, it is used extensively in the automotive industry to replace metal parts. LFTs are popular because they are compatible with existing machinery for processing Short Fibre Thermoplastics (SFT). This makes them a simple way to improve material properties at a modest cost increase.

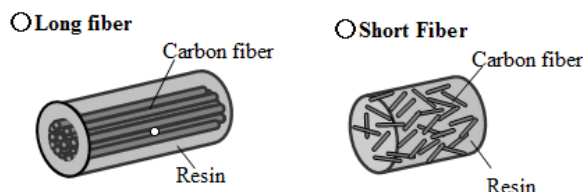


**Figure 2.9:** Illustration of fibre fillers in long vs short fibre pellets. Long fibre pellets contain fibres that run the entire length of the pellet, short fibre pellets contain fibres much shorter than the pellet <sup>4</sup>

LFT pellets are created by pultruding continuous fibres through an impregnation die full of liquid resin before being cooled down and cut to length by a pelletiser. This process is illustrated in Figure 2.10 and results in pellets containing fibres that run the entire pellet length. As shown in Figure 2.9, this differs from SFT pellets which contain shorter fibres which are randomly distributed inside the pellet.

LFT pellets are industrially used in injection moulding. However, despite being injected through narrow mould cavities, fibres are not shear aligned to a great degree. This is evident in the achieved properties seen in Figure 2.11a and Figure 2.11b. Notably, injection moulded LFT does not achieve significantly higher strength or stiffness in flow direction than SFT. Instead, they improve off-axis properties and toughness, as well as properties when heated above the glass transition temperature.

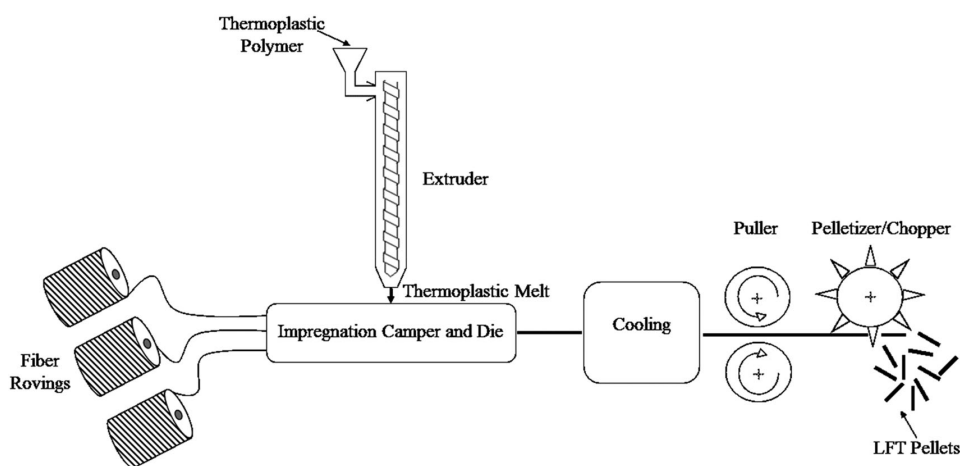


**Figure 2.10:** Long fibre pellet manufacturing by pultrusion process, fibres are impregnated in resin, pultruded, then pelletised to length [19]

<sup>4</sup><https://www.toray.jp/plastics/en/torayca/index.html>

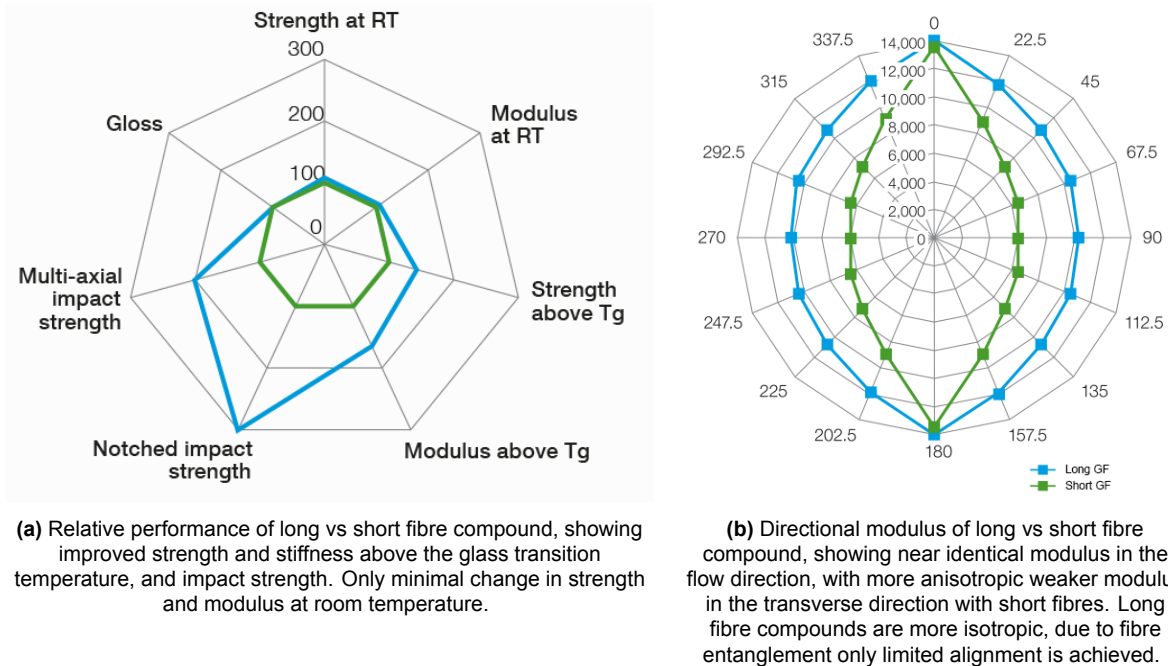


**Figure 2.11:** Overview comparison of long (blue) vs short (green) fibre compound [20]

While the LFT fibres that align contribute better than aligned SFT fibres, the lower degree of alignment means fewer fibres are aligned with the stress. However, this lower degree of alignment contributes to a higher degree of isotropy, which is useful when producing metal-replacing parts. Mould and part-design work is simplified when flow direction through the mould does not affect directional material strength significantly. This can be a problem with SFT as can be seen in Figure 2.11b, parts that are considerably weaker in transverse-to-flow direction while this effect is significantly reduced with LFT.

It is also known that fibre attrition is relatively high in injection moulding [21, 22, 23, 24]. Fibres break due to being bent by resin flow upon mechanical contact with screw extruder walls and contact between fibres while being processed inside the screw extruder. Further fibre length attrition occurs during injection moulding, as significant shearing occurs against mould walls.

### 2.3.1. Long-fibre extrusion for additive manufacturing

An extreme die-swelling phenomenon was observed with LFT pellets extruded with the CEAD screw extruder. Extrudates expanded to double the nozzle diameter or more, implying a void content of 75% when the cross-sectional area's expansion is considered. These expanded extrudates have a rough fibrous outer texture as shown in Figure 2.12 and are extremely porous.

No mention of a similar phenomenon with long fibres was found in the literature, as LFT additive manufacturing has not been widely studied. Additive manufacturing imposes different requirements than traditional processes which use LFT. In moulding processes, which is the chief use case of LFT, the melt is constrained by pressure from thin mould cavities, which restrict and hold the extrusion into shape until it solidifies. In die-extrusion processes, the extrusion is cooled as it exits the die to solidify

and secure the extrusion to the desired shape, which also prevents expansion.



**Figure 2.12:** 12 mm fibre pellet extrusion test, showing fibrous exterior and large cavity caused by fibre/matrix separation from swelling

However, in additive manufacturing the extrusion is not confined. Instead, the material is simply deposited on previous layers. Also, the temperature must be high enough to allow reptation between polymer molecules of the new and previous layers to ensure good bonding. However, this high-temperature molecular mobility also lowers the melt strength of the polymer, which, together with the freedom to expand, allows the extrudate to swell freely and expand. Therefore this problem seems unique to additive manufacturing, and a solution is required.

## 2.4. Thesis Definition

For AM to compete and grow in the end-use product market, processes using stronger materials must be developed. For LSAM, the use of LFT is a promising but unexplored way to improve the mechanical performance of large printed parts.

While LFT use is already established and growing in the injection moulding industry, the lack of shaping freedom and restrictions of injection moulding limit the ability to achieve and control the alignment of fibres. If long fibre length and alignment can be achieved, the high shaping freedom of AM could result in unprecedented high-performance parts at an economical price. However, there is a knowledge gap in both literature and practice in using long fibre compounds for additive manufacturing. While short and continuous fibre printing has already been developed and commercialised, 3D printing with long fibre thermoplastics remains unexplored.

***This thesis aims to investigate the viability of LFT as feedstock material for FGF additive manufacturing and demonstrate that higher specific strength is achievable through the use of longer fibres.***

An extreme swelling phenomenon currently makes LFT unusable for additive manufacturing. Therefore, this swelling phenomenon will be investigated. The first steps will determine the cause of the swelling, then test which methods may be effective in aligning fibres and solve the swelling to make the material processable. Additionally, the mechanical performance of long-fibre extrusions needs to be quantified, assessed and compared to currently used short-fibre compounds.

## Experimental Setup

This chapter describes the equipment, materials, testing methods, microscopy image processing procedures and mechanical testing used for experimentation and to acquire the results in this thesis.

### 3.1. Screw Extruder

The CEAD E-25 Robot Extruder is a single screw 25 mm barrel screw extruder with four individually controllable heating zones, a representative diagram of which is given in Figure 3.1. Material is fed into an opening at the top of the extruder through a hopper, where a rotating screw feeds the material down. Heated walls and shearing action from the rotating screw heat and mix the resin pellets. The gap between the barrel and the screw shaft narrows, this constriction in space causes compression of the resin pellets, densifying the melt, squeezing out air and building up extrusion pressure. Finally, the extruder terminates in a nozzle holder capable of mounting nozzles of various diameters.

The controllable inputs of the screw extruder are the nozzle size, RPM setpoint for the screw extruder's servo motor and temperature setpoints of the four barrel heaters. The four temperature setpoints are given in the format:

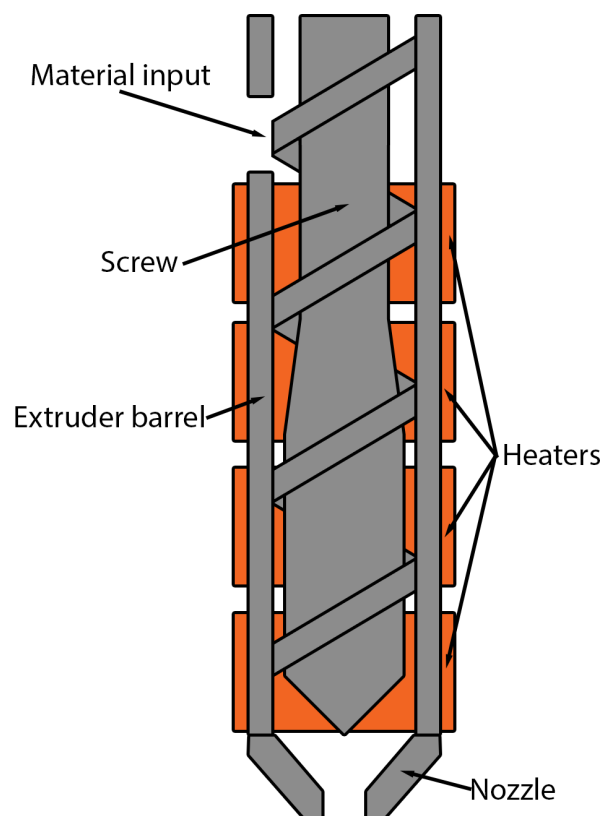


**Figure 3.1:** Anatomy of a screw extruder, consists of a barrel with four heating zones, a rotating screw which pushes and compresses material downward, pressurised molten resin exits downward through the nozzle

190/200/220/205, which are the material transport zone, compression zone, metering zone and nozzle zone setpoint temperatures in °C, respectively.

### 3.1.1. Material used

Polypropylene (PP) pellets containing 30% long glass-fibre filler (LGFPP) in three lengths were provided by Solvay AM. Polypropylene containing 30% short glass-fibre (SGFPP) from CEAD and High-Density Polyethylene (HDPE) from SABIC were used as testing materials. These materials are listed in Table 3.2. Drying is not typically required for PP as it is not a hygroscopic material, but all material was dried anyway as a precaution.

	W/W% GF	Fibre length	Resin	Melt Temp
	0%	-	HDPE	132°C
SGFPP	30%	0.2mm	PP	170°C
LGFPP	30%	7mm	PP	165°C
LGFPP	30%	9mm	PP	165°C
LGFPP	30%	11mm	PP	165°C

**Table 3.2:** Fibre content, lengths and resins in pellets used



**Figure 3.3:** 11 mm LGFPP pellets, 1 euro coin for scale

## 3.2. Extrusion Analysis

Samples for analysis were produced by free air extrusion, allowing them to cool before cutting them. The extruder was purged between every sample to avoid sample contamination. These samples were measured for swelling, fibre length and orientation analysis, and mechanical testing.

### Cross-sectional area

As excessive swelling was the main challenge, a simple way of measuring and calculating the swelling relative to the nominal nozzle orifice had to be devised. To do this, the 'swell ratio' was measured by calculating the cross-sectional area of the extrusions and dividing them by the cross-sectional area of the nozzle orifice.

The extrusion area was calculated by measuring the feret ( $D_{max}$ ) and minimum feret diameters ( $D_{min}$ ) of the extrusion with callipers at  $n$  number of spots along an extrusion. Then, assuming an elliptical shape, the ferets were used as the major and minor axes. The average of these areas was taken and divided by the nozzle CSA to yield the 'swell ratio' as shown in Equation 3.1. This swell ratio was used as a quick way to evaluate progress, with the goal of achieving no swelling, with a ratio close to 1.

$$swellratio = \frac{\sum_{i=1}^n D_{max,i} D_{min,i}}{n D_{nozzle}^2} \quad (3.1)$$

### Fibre length measurement

As increasing the fibre length of printer extrusions is the objective of this thesis, it was also essential to evaluate the fibre length of extrusions and determine how modifications were affecting fibre attrition and final fibre length distribution (FLD)

Samples for FLD analysis were prepared by cutting extruded samples. Samples were cut at a length at least triple the maximum fibre length to avoid sampling fibres damaged by the cutting process. The samples were calcined in a furnace at 600 °C for 1 hour (with a half-hour ramp up) to remove the matrix and leave bare fibres, as can be seen in Figure 3.4.



(a) Samples before calcination, black due to pigmentation in PP resin



(b) Samples after calcination, the resin has been removed, revealing bare glass-fibres

**Figure 3.4:** Calcination of printed samples, long fibre pellets and short fibre pellets

Bare fibres were extracted from the centre of samples with forceps, special care was taken to minimise disturbance of fibres, and especially avoid losing small fibre dust. However, it should be acknowledged that there is always selective bias when manually extracting fibres by hand. These fibres were suspended in pure ethanol, spread over a large Petri dish, and dried in a vacuum oven. Ethanol was selected for having a low viscosity, allowing even fibre dispersion and leaving minimal residue after drying.

These Petri dishes with fibres were analysed by microscopy, recording stitched images with a Keyence VR-5000 Wide Area 3D Measurement, then processed with the 'Ridge Detection' [25] plugin to detect and measure the fibre lengths with Fiji [26], an example of which is shown in Figure 3.5. These lengths were collected into a histogram, and the

number average  $l_n$  and weight average  $l_w$  were calculated according to Equation 3.2 and Equation 3.3 [6].

$$l_n = \frac{\sum_{i=1}^n N_i l_i}{\sum_{i=1}^n N_i} \quad (3.2)$$

$$l_w = \frac{\sum_{i=1}^n N_i l_i^2}{\sum_{i=1}^n N_i l_i} \quad (3.3)$$

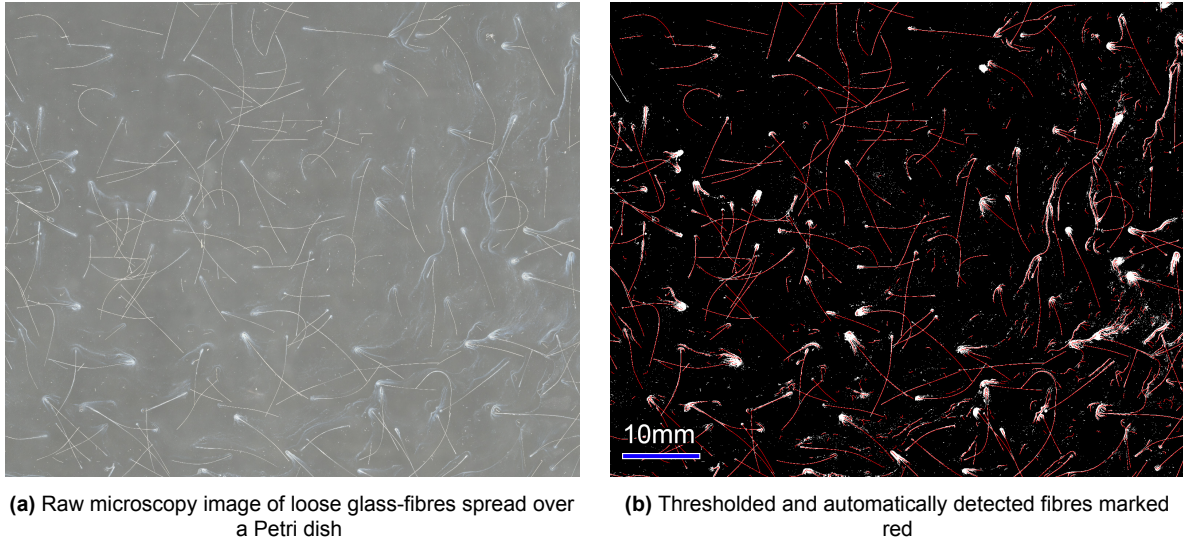


**Figure 3.5:** ImageJ automatic fibre length detection after microscopy of calcination to expose fibres

### Fibre content measurement

The fibre weight fraction (W/W%) was measured by ASTM standard D 2584 [27]. This method involves measuring the mass of a composite sample before and after calcination. The ignition loss mass is considered the resin mass, the remaining mass is assumed to be pure fibre. The fibre weight fraction can then be calculated with these two masses. Samples were dried in a vacuum oven to remove all moisture inside the resin before weighing.

### Void content measurement

Void content of samples was determined by Method II of ASTM standard D 3171 [28]. This method involves weighing and measuring samples to calculate their density. The more accurate method of measuring the volume of the samples such as submersing the sample in liquid was not viable as the material was so porous. The porosity would result in the liquid penetrating the sample and the low density of samples would result in problems due to floating. Therefore, samples were measured with calipers and their volume was calculated. The void content was calculated by weighing them and then comparing the density to the density and content fraction of resin and fibre.

### Fibre orientation measurement

To evaluate the degree of fibre orientation in samples, the fibre angles can be collected into a fibre orientation distribution (FOD) histogram. A sample is planed, polished, and observed with microscopy to measure the ellipticity of fibre cross-sections. By measuring the semi-minor ( $D_{min}$ ) and semi-major ( $D_{max}$ ) axes of fibres and assuming the fibres are perfectly round, the deviation angle from normal  $\phi_n$  of the fibre from the plane normal can be calculated according to Equation 3.4.

$$\phi_n = \arccos \left( \frac{D_{min}}{D_{maj}} \right) \quad (3.4)$$

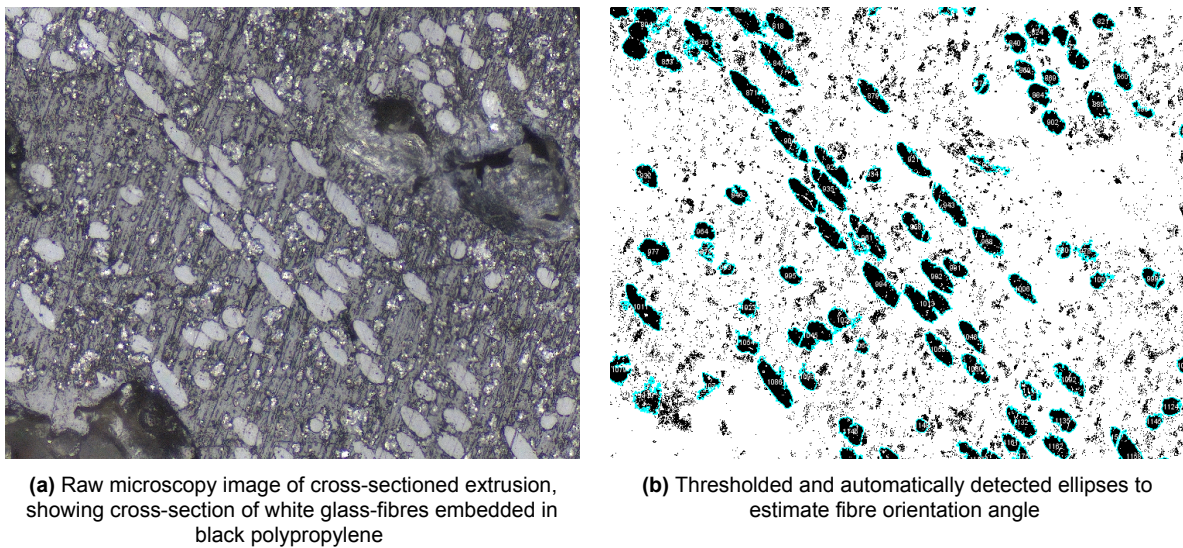


**Figure 3.6:** ImageJ automatic fibre orientation measurement of a polished cross-section of extrusion

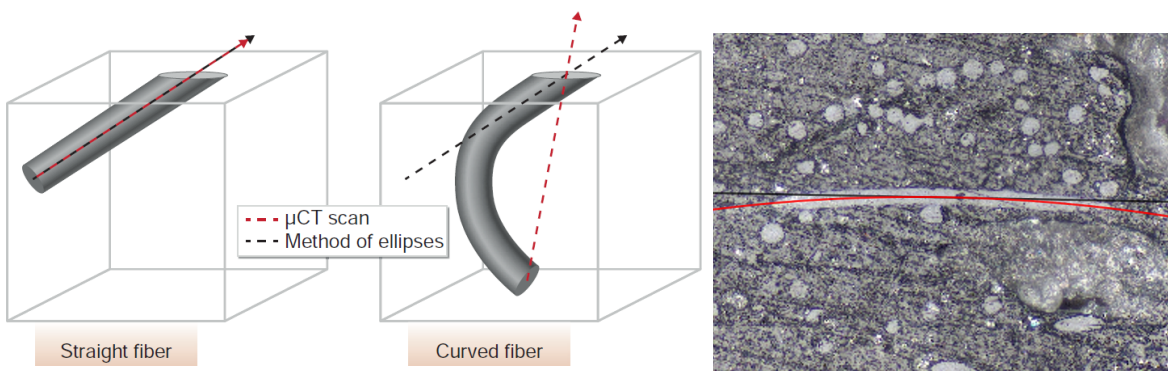


**Figure 3.7:** Method of Ellipses, estimating fibre angle by measuring cross-sectional ellipticity. This method works with straight fibres, but as long fibres can be curved, it fails to capture the curvature or direction for the entire fibre [6]

**Figure 3.8:** Cross-section of a curved fibre, with lines showing a straight and curved path

To prepare microscopy samples, extrudates were cut with a diamond saw. These samples were then sanded and polished at increasing grit. These polished samples were observed with a Keyence Laser Scanning Confocal Microscope. After threshold-

ing to separate the fibre from the matrix in images, ImageJ was used to automatically detect fibre cross-sections as ellipses as shown in Figure 3.6.

The method of ellipses has several key limitations, especially for analysing long fibres. The issue stems from the method's reliance on measuring the cross-sectional fibre angle. While this may accurately describe a short, stiffer fibre, a longer fibre is more flexible and cannot be assumed to be straight throughout. This problem is illustrated in Figure 3.7. Another issue is that a fibre may be curved sideways (with an out-of-plane axis of curvature), then the cross-section will not appear elliptical, an example of this is shown in Figure 3.8.

Finally, it must be noted that fibre orientation was measured in free extrusion samples, as depicted in Figure 3.9a, which unfortunately is not representative of fibre orientation after 3D printing. Figure 3.9b shows material being built up in the layer-by-layer fashion typical of 3D printing. This process deforms the extruded material, shearing it against previously extruded layers into a fixed layer height. Fibre orientation will be affected by this deformation, possibly in a positive way but this was not investigated.

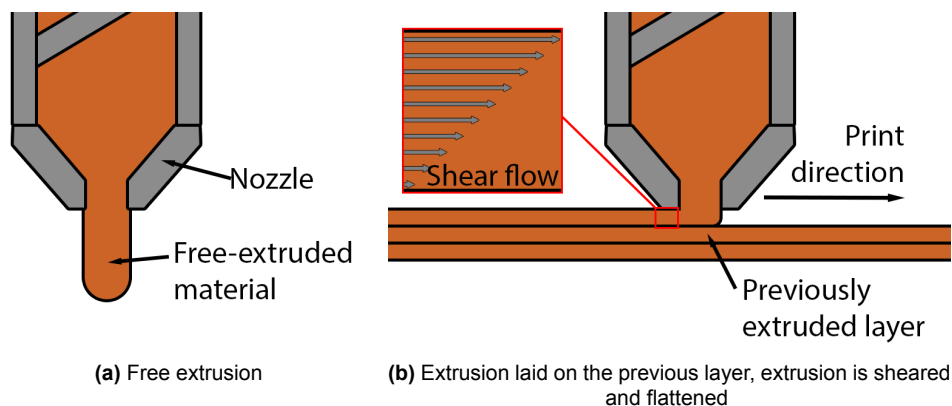


**Figure 3.9:** Deformation of extruded material when sheared against previous layer instead of freely extruded

### 3.3. Mechanical Testing

Three-point bending testing was used to evaluate the flexural strength of extruded samples. A Zwick 20 kN standing mechanical testing machine was used with a 1 kN load cell. Samples were placed between the three-point bending setup shown in Figure 3.10, which has 10 mm diameter end supports placed 120 mm apart and a 20 mm diameter indenter. The load was applied by the indenter at a rate of 1 mm/min.

The main reason for using three-point bending was to avoid the complexity of attempting to clamp irregular, round samples. However, the shape of the samples still caused some issues, as they had elliptical cross-sections with undulating variation in thickness. To account for the elliptical cross-section, the minor and major axes at the centre of each sample were measured with callipers to calculate the second moment of area. Samples were placed in the bending setup so as to align the major axis with

the bending plane. This was considered valid as each sample failed at the centre point below the indenter.

The breadth-to-depth ratio ranged from 10 to 20 across all samples with the exception of original LGFPP samples, which had the highest degree of expansion. These samples had a ratio of 5. Therefore the testing of these samples likely deformed by shearing instead of pure bending. Also, as the shape of the sample was rounded, contact by the round (but perpendicularly placed) indenter would create a pressure point which would cause some indentation by crushing. This inflates the displacement and reduces the effective thickness of the tested material, especially on the softer, more porous samples. This effect is visible in stress-strain curves by a reduced stiffness gradient at the beginning of some of the more porous samples.

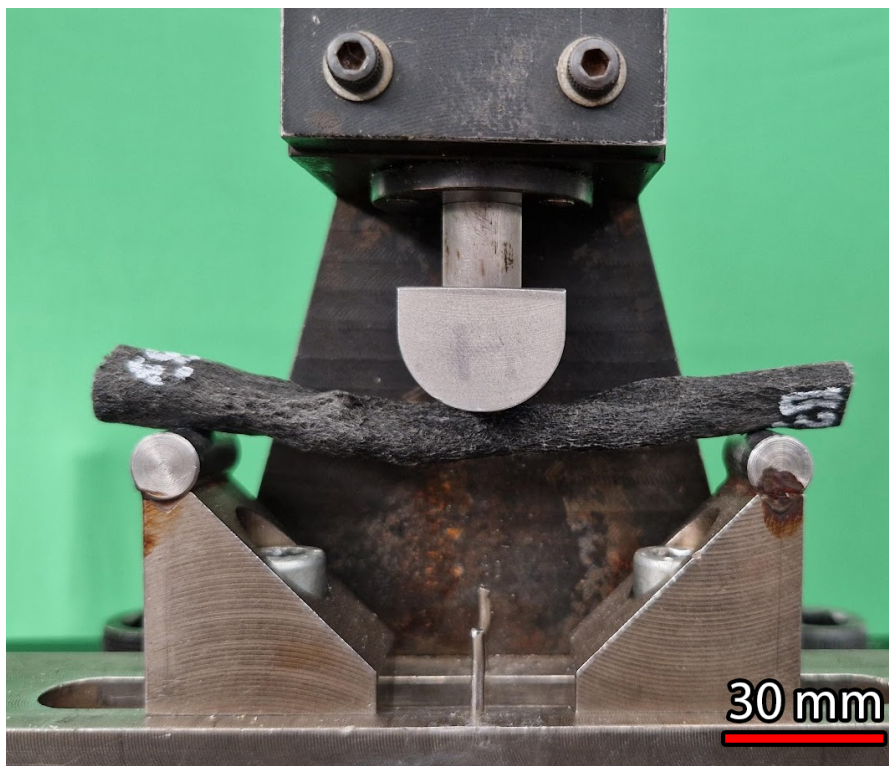


**Figure 3.10:** Three-point bending mechanical test setup, 10 mm diameter end supports 120 mm apart, 20 mm diameter indenter



## Initial Investigation

The extreme swelling phenomenon is hypothesised to be caused by fibre misalignment, and aligning the fibres would solve the swelling and visa versa. This chapter describes the investigation into the cause of swelling and initial attempts to align the fibres.

### 4.1. Conventional Polymer Die-swell

Die-swell, or the Barus effect, is where the extruded material swells to a diameter larger than the nozzle [30, 31, 32]. It is caused by the visco-elasticity of polymers, as the melt is forced into a contracted nozzle throat, the flow accelerates by elongating, as shown in Figure 4.1. This temporarily stresses and elongates the polymer molecules, which release this stress at the die-exit by returning to their original shape, causing the extrudate to expand sideways.

The Barus effect, however, is not a satisfactory explanation for the LFT expansion as it does not correspond to several die-swell characteristics. Die-swell develops sideways by length-wise contraction, [33] which preserves material volume without resulting in porosity. It develops quickly, most of the swelling occurring directly at the die-exit [34]. And die-swell also traditionally decreases with increasing fibre fraction and length as the fibres resist the polymer's tendency to swell [35] and typically reduce with increased extrusion temperature [36, 37, 38].

In contrast to these characteristics, the long-fibre swelling is associated with high

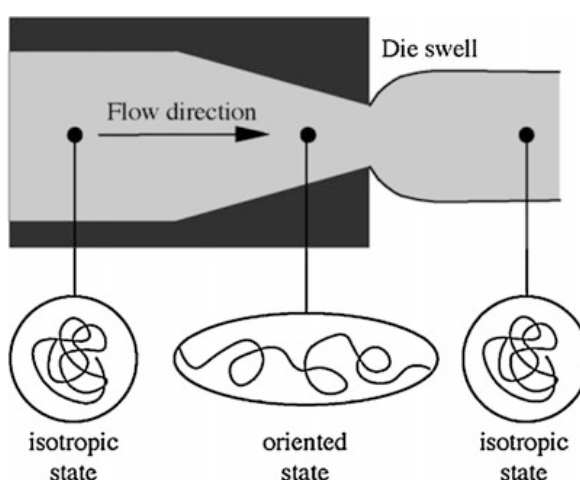


**Figure 4.1:** Die swell due to polymer elasticity, energy stored in polymer molecules as they were deformed and compressed through a convergent die channel being released as swelling on die-exit, as the molecules relax and return toward their initial state [29]

porosity, as seen in Figure 4.2 and is slow to develop as shown in Figure 4.4, the swelling develops some distance away from the nozzle as it takes several seconds to expand fully. It also increases with nozzle temperature, as shown in Figure 4.3.

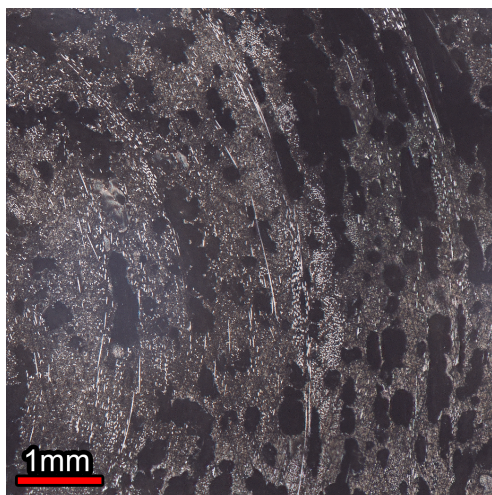


**Figure 4.2:** Sectioned microscopy of original long fibre extrusion with high swelling, showing high porosity

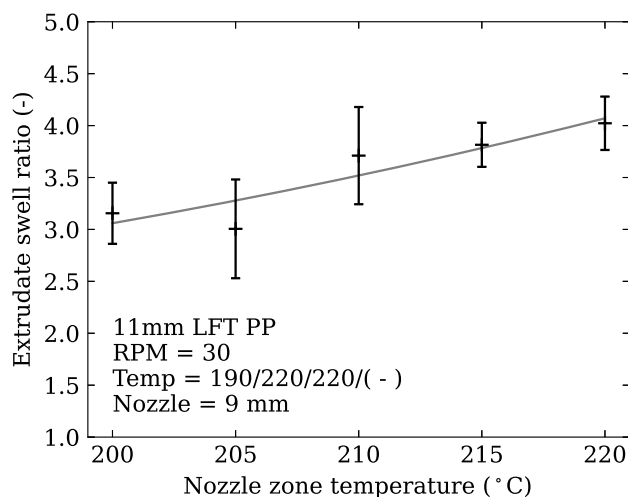


**Figure 4.3:** Extrudate swelling at nozzle temperature settings 200-220°C, swelling increases with increased nozzle temperatures

Instead, the long fibres themselves are suspected of causing the swelling. The swelling seems to be opposed by the polymer in the melt rather than being the cause of it. The swelling increases with time and with higher nozzle temperature as it only stops once the polymer cools and solidifies. Hotter resin has lower melt strength and viscosity, tearing more easily and expanding more quickly. The porosity occurs due to tears created in the polymer by fibre swelling.

## 4.2. Fibre/Nozzle Interaction

The discrepancies between the observed LFT swelling from known polymer die-swell lead to the belief that the long fibres cause the swelling. It was hypothesised that the fibre polymer melt and the nozzle interaction were the cause. Extraction tests were performed with different input fibre lengths and nozzles to explore this.

The results of the fibre length test are displayed in Figure 4.5, together with a baseline point for normal short fibre extrusion. It was expected that a slightly lower fibre length could result in a massive improvement in swelling reduction, and as previously shown in Figure 1.5, even a fibre length of 4-5mm is capable of significant mechanical performance. However, experimentation with 7, 9 and 11mm fibres showed that the reduction in swelling was not as high as hoped for. Long fibres would have to be abandoned to have an acceptable reduction in swelling, which defeats the point of this project.

Instead of lowering the input fibre length, variation of the nozzle diameter was trialled as an attempt to lower the effective fibre/nozzle ratio. An inverse relationship between nozzle diameter and the swell ratio was observed, shown in Figure 4.6. It was also



(a) Extruded material swells as it gets farther away from the nozzle

(b) The same extrusion 10 seconds later, the swelling has fully developed up to the nozzle

**Figure 4.4:** Extruded long glass fibre polypropylene material showing swelling behaviour

found that extrusion with the largest 15 mm nozzle had the lowest variance in swell diameter, suggesting more stable, consistent processing, which is attractive for good print quality. It should be noted that there is a region before the nozzle with a diameter of 20 mm, and the test shows that the swelling would disappear close to this value.

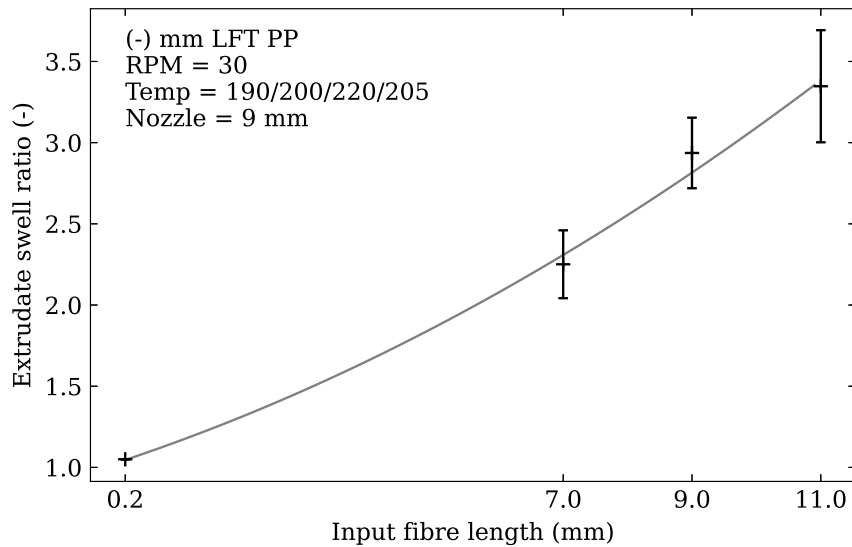


**Figure 4.5:** Extrudate swelling increased with increased input fibre pellet length

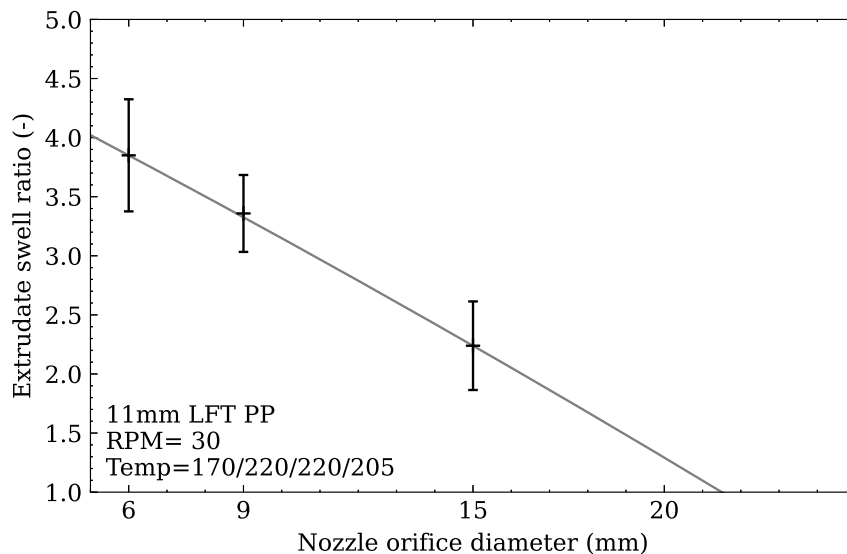


**Figure 4.6:** Extrudate swelling increases with smaller nozzle size

These tests show a strong correlation between the fibre: nozzle ratio and the swell ratio. This suggests the swell ratio is caused by something that happens to the fibre/polymer melt as it passes through the nozzle. It is believed that the cause is another type of die-swell, not caused by the stressing of polymer molecules being temporarily aligned by stress as discussed in the previous section, but by an entangled network of fibres. This phenomenon was not found in the literature. Similar to the polymer die-swell shown in Figure 4.1, it is believed that the fibre network is being compressed as

it passes through the constricted nozzle, storing potential energy by bending fibres. These fibres release this energy upon exiting the nozzle by straightening, causing the fibre/polymer melt to expand.

### 4.2.1. Fibre entanglement

An entangled fibre network is a characteristic of LFT in screw injection moulding. An example is shown in Figure 4.7. This entangled fibre 'skeleton' has the advantage of having high isotropy due to unaligned fibres. This makes the material easier to use when replacing metal parts[39, 20, 40].



**Figure 4.7:** Injection moulded long fibre thermoplastic part, with fibre 'skeleton' visible on the left, exposed by pyrolysis <sup>1</sup>

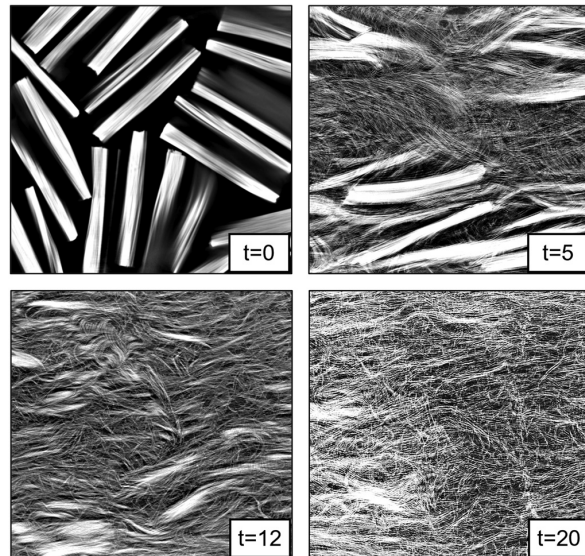


**Figure 4.8:** micro CT slices of LGFPP40% fibre loading exposed to a shear flow for different residence times [41]

The entanglement occurs due to the shear mixing of fibres inside the screw extruder. Figure 4.8 shows the entanglement that occurs after LFT pellets are exposed to shearing. Long strings tend to form knots spontaneously [42], and in the case of LFT, the fibre length also causes fibres to interact with each other.

$$V_f < \left(\frac{d}{l}\right)^2 \quad (4.1) \quad \left(\frac{d}{l}\right)^2 < V_f < \left(\frac{d}{l}\right) \quad (4.2) \quad V_f > \left(\frac{d}{l}\right) \quad (4.3)$$

The effective concentration of a fibre solution depends not only on the fibre content but also on the length of the fibres. This relationship is shown in equations (4.1) to (4.3) and plotted in Figure 4.9. They delineate the dilute region (where fibres are not expected to make contact with each other while rotating), the semi-concentrated region (where occasional contact is expected) and the concentrated region (where contact becomes unavoidable due to the long fibre length). For reference, the fibre concentration and approximate lengths are also marked in the figure.

<sup>1</sup><https://www.plasticomp.com/long-fibre-benefits/>

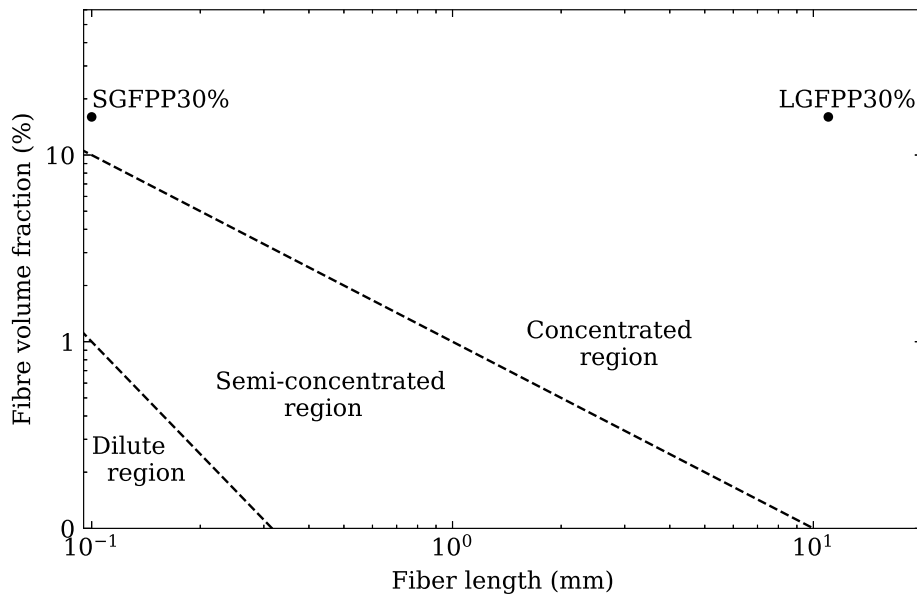


**Figure 4.9:** Fibre-fibre interaction regions, delineated by functions of fibre concentration and fibre length, in the concentrated region, fibre-fibre interaction is inevitable. 30% long glass fibre polypropylene (LGFPP30%) is deep in the concentrated region

The increased fibre length in LFT places them far into the concentrated region, and it can be expected that fibre-fibre interaction during mixing is unavoidable. This contact can cause fibres to break or entangle [43, 19, 44], restricting their ability to continue aligning with the shear field.

### 4.3. Ineffectiveness of Traditional Fibre Alignment

Due to the fibre entangling, the fibre orientation is expected to be poor. It was assumed that the two go hand in hand; poor alignment causes entangling, preventing alignment. However, this section will explain why correcting this problem is not trivial.

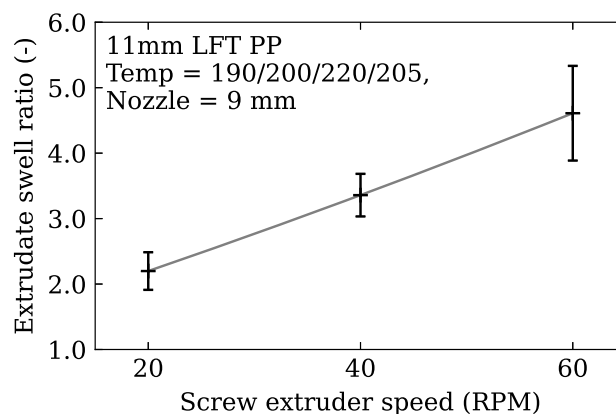


**Figure 4.10:** Extrudate swelling increases with increasing screw RPM, which increases shear rates in the screw extruder and also at nozzle flow

Tests with varying RPM, Figure 4.10, showed that swelling was aggravated at higher processing RPM. Higher RPM leads to faster shearing between the screw and barrel

walls and faster flow through the nozzle, which also increases shear rates. Higher shear rates did not seem effective at aligning fibres and reducing the swelling. This is partly believed to be because of the entangling of long fibres previously discussed but also because the fibres are too long to be shear aligned.

Shear alignment occurs when a velocity gradient field develops. The laminar flow will develop a velocity gradient due to velocity being minimum (modelled as 0 with the no-slip condition) at the walls due to friction and maximum velocity at the centre of the flow. The simplified 2D planar flow is shown in Figure 4.11.

A differential flow field causes any fibres not aligned with the flow direction to experience a pitching moment due to the difference in flow velocity experienced across its length, which will align the fibre with the flow. This is shown on Figure 4.11 with the blue fibre. Due to the parabolic shape of the field, the velocity gradient and fibre alignment are highest near the nozzle walls.

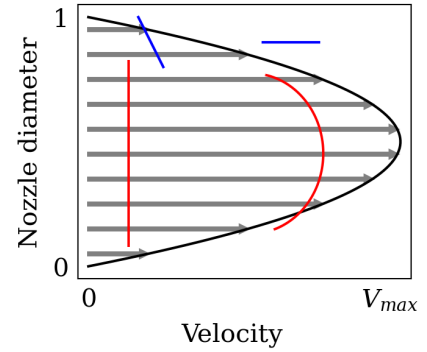


**Figure 4.11:** Simplified parabolic shear flow, short blue fibre being aligned, long red fibre being bent by shear flow as a bending moment rather than a rotating moment is applied

$$\dot{\theta} = \frac{\gamma}{\left(\frac{L}{d}\right)^2 + 1} \left( \left(\frac{L}{d}\right)^2 \sin^2 \theta + \cos^2 \theta \right) \quad (4.4)$$

As shown in Equation 4.4, the angular velocity of fibre alignment  $\dot{\theta}$  [45, 46] is dependent on the shear rate of the flow  $\gamma$ , the aspect ratio of the fibre ( $L/d$ ) and  $\theta$ , the fibre angle away from the parallel flow. The angular velocity is near constant and insensitive to fibre aspect ratio (at high values of aspect ratio), this is due to the increased moment being applied to the longer fibre being counteracted by the longer fibre having more rotational inertia and drag through the viscous matrix material. However, this theory makes two assumptions which do not apply to long fibre extrusion.

As fibres get longer and approach the diameter of the nozzle, it can no longer be assumed that the fibre will be affected by one shear gradient. Instead, by being exposed to two gradients, a bending moment is applied to it rather than a rotational one; this is illustrated on Figure 4.11 with the red fibre.

$$S_{eff} = \frac{E\pi}{64\eta_m\gamma\left(\frac{L}{d}\right)^4} \quad (4.5)$$

Also, the effective stiffness of a fibre being sheared in a fluid matrix is highly dependent on the aspect ratio  $L/d$  as shown in Equation 4.5 [47, 48], where  $E$  is the fibre Young's modulus,  $\eta_m$  is the matrix viscosity,  $\gamma$  is the shear rate, and  $L$  and  $d$  are the length and diameter of the fibre. The decrease in fibre stiffness with increasing fibre length results in a tendency for fibres to bend rather than rotate into alignment.

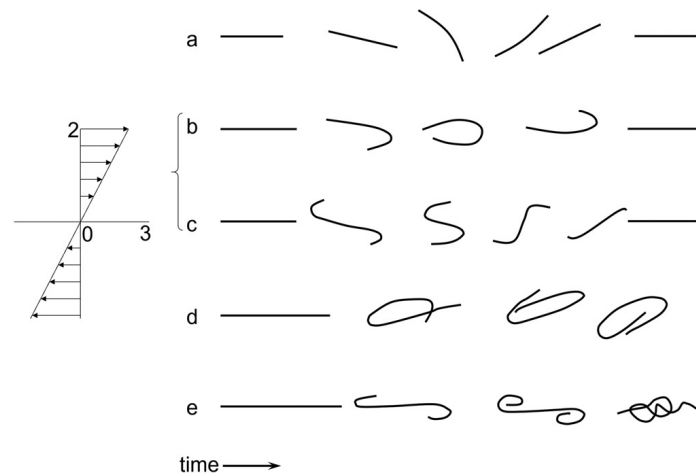


**Figure 4.12:** Types of fibre motion in a Couette velocity flow field. a. springy rotation, b. single-ended snake orbit, c. double-ended snake orbit, d. coiled rotation, e. coiling with entanglement. Shear alignment is only effective on shorter stiff fibres, longer fibres are too flexible, bending and entangling rather than being rotated [49]

This challenge in attempting to align too long fibres is illustrated in Figure 4.12, which sketches the behaviour of various single fibres in a gradient velocity field. When a very long fibre is exposed to a flow gradient, the shear forces along the length of the fibre cause the fibre to locally bend the tips and coil the fibre rather than rotating the entire fibre the way it does for shorter fibres. In extreme cases, the fibre coils completely into a so-called ‘snake-orbit’ or forms a knot by itself.

## 4.4. Reducing Residence Time

As too much mixing of the long fibres seems to result in entanglement and therefore swelling, an attempt was made to reduce the residence time and the duration of time fibres spend inside the extruder. Increasing RPM is one way to decrease residence time, but the increased shear rate showed increased swelling in Figure 4.10. Another available process parameter that would achieve shorter residence time is to reduce the material transport zone temperature, which is the first zone as shown in Figure 4.13.

As this zone determines the rate of heating the pellet for melting, it determines how quickly the resin melts and fibres are released. Traditional LFT processing recommends heating the pellets as quickly as possible to reduce fibre breakage. However, by keeping the temperature low, the resin melting can be delayed, which delays the release of fibres, artificially shortening the screw extruder length. Figure 4.14 shows

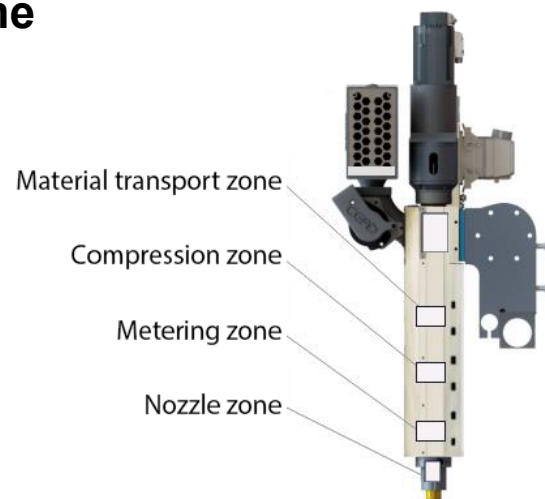


**Figure 4.13:** The four individually temperature controllable zones of the CEAD E-25 extruder, the material transport zone is the first zone to heat pellets

a mild and insufficient effect on swelling. Even lower temperatures were attempted, but this caused the extruder motor torque limit to be exceeded as the resin became too viscous.

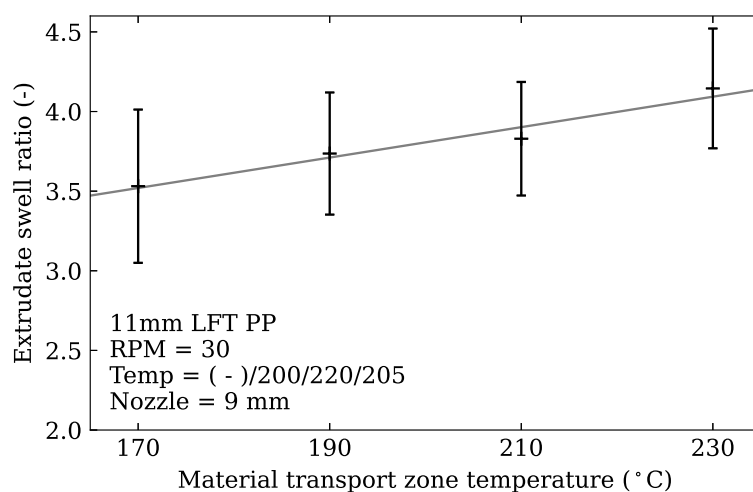


**Figure 4.14:** Extrudate swelling decreases at lower transport temperature settings

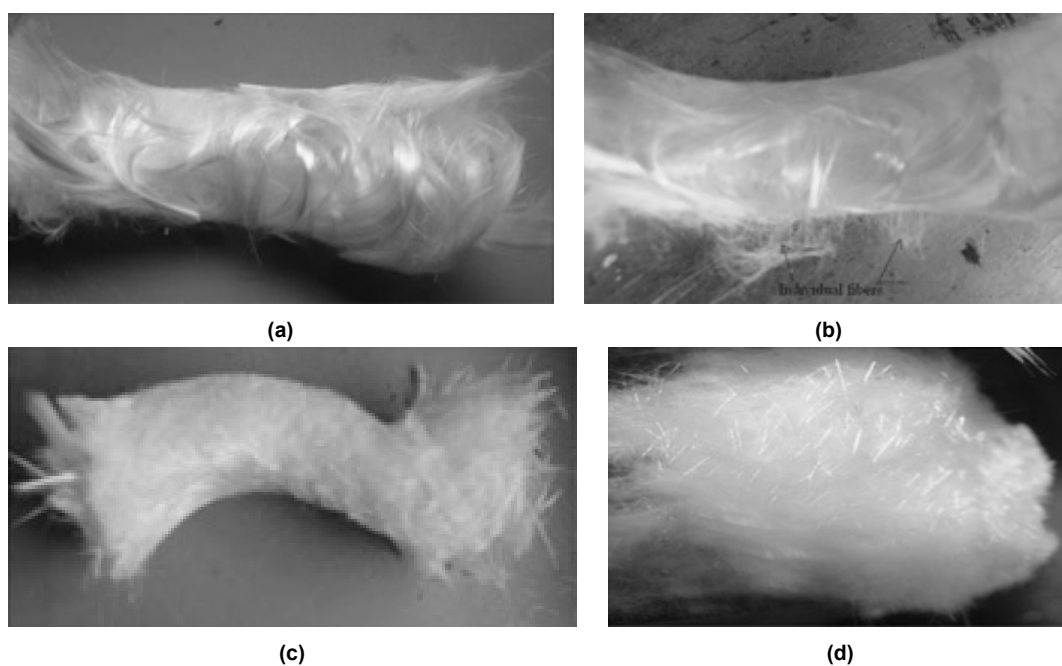


**Figure 4.15:** Fibre morphology of long GF PP collected progressively along screw extruder, exposed by matrix burning [23]. Shows progressively higher degree of fibre dispersion, shortening and entangling

Resin/fibre morphology within a screw extruder is typically investigated by freezing the resin and pulling the screw out of the extruder [50, 21, 51, 52]. This allows samples to be taken at various points of the extrusion process for analysis. Unfortunately, attempts to examine the material along the extruder's inside by cold screw pull-out were unsuccessful. The high viscosity of the long fibre reinforced resin and the fibre's

grip on the screw was too strong. Even after increasing the temperature setpoints to 400°C and waiting for the resin to soften and pulling with a winch, the screw could not be pulled out. The pull attempt was abandoned when the resin began to smoke heavily.

Ren et al., [23] however, successfully performed a long GF PP screw pull-out and took samples at progressively deeper flights of the screw. Images of these samples after resin removal are shown in Figure 4.15. These images show a progressively higher degree of fibre dispersion and entangling. By delaying fibre release by lowering the material transport zone temperature (as shown in Figure 4.14), the fibre state is believed to be at an earlier stage of mixing when the nozzle is reached.

# 5

## Hetero-phasic Pellets for Pre-alignment and Lubrication

Investigation in the previous chapter led to the conclusion that conventional strategies were simply ineffective at solving the swelling due to the processing difficulties of long discontinuous fibres. This chapter describes a new method devised to solve the swelling phenomenon and presents the properties of the long-fibre blended resin material.

### 5.1. PP/PE blend

Previous testing of the first temperature zone (Figure 4.14) showed a mild but promising reduction in swelling with lower temperatures. To further explore this effect, HDPE pellets were mixed in with the 11 mm LGFPP pellets (Figure 5.1) to act as lubricants. HDPE (with a melting temperature of 132°C, 40°C lower than the PP resin) was expected to melt while the LGFPP stayed solid. This was expected to lower the effective temperature of the overall resin as a significant amount of heat inside a screw extruder can come from the friction from shearing rather than the supplied heat. By introducing a lubricant and reducing this friction, it is believed the PP will stay cooler and the fibre release delayed.

The addition of PE to PP has already been studied and is a common way of tailoring the strength, stiffness and toughness of PP. Generally, the addition of the weaker HDPE



**Figure 5.1:** Mixed pellet input, black long glass fibre polypropylene pellets with lower temperature melting white HDPE for lubrication

lowers the strength and stiffness of PP while increasing toughness. However, under elongational flow (as is the case in the nozzle), the strength of the blend increases and peaks at 10% PE but decreases with increasing PE content [53], the increase in properties is due to strain hardened, elongated HDPE particles (due to elongational flow) increases the crystallinity of PP [54]. While polymer die-swell increases with the addition of PE in the case of neat resins [55], the fibre die-swell of LGFPP seems to be significantly reduced by PE.

The HDPE/LFT blend was extruded with a material transport temperature of 170°C. Different fractions of HDPE additive were trialled, and the resulting reduction in swelling is given in Figure 5.2 and a comparison is shown in Figure 5.3.

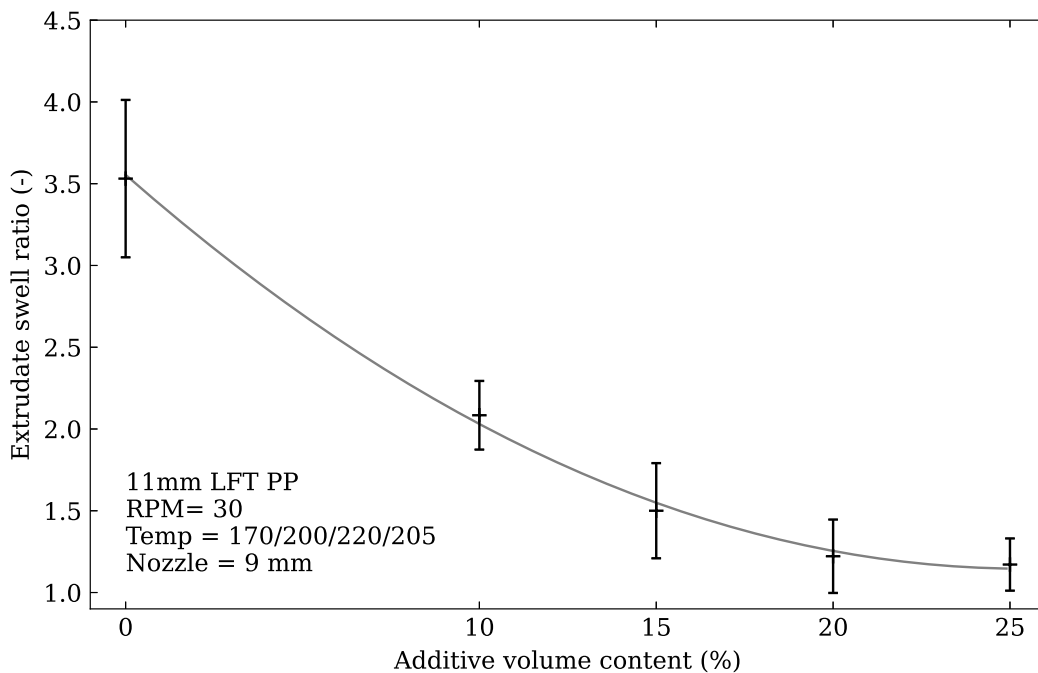


**Figure 5.2:** Extrudate swelling is lowered dramatically with the addition of lubricating additive content

### 5.1.1. Printability

It was previously impossible to print with the original material as the extruder would crash into previously deposited layers which had expanded upward to block the tool path. Figure 5.4 shows a print test performed to show that the reduction in swelling with the LGFPP/PE blend is sufficient to allow material to be deposited in subsequent layers. The surface has a rough, fibrous exterior, with fibre bundles occasionally pulled out of extrusions. This was caused as the nozzle moved while depositing material. As the material is sheared, entangled fibres would be pulled out as fibres slide across each other.



(a) Original 11 mm long fibre extrusion showing a high degree of swelling

(b) 25% HDPE blended 11 mm long fibre extrusion showing elimination of swelling

**Figure 5.3:** The dramatic effect of HDPE on swelling reduction



(a) Top view



(b) Side view

**Figure 5.4:** Printed layers with 15% modified LGFPP. Beads 3mm high, 20 mm wide

## 5.2. Working Mechanism

PE has a lower viscosity than PP, and the addition of PE into PP reduces the viscosity of the blend. The hypothesis that the melt was behaving differently simply due to lower resin viscosity was tested using a higher temperature profile of 190/200/220/205. This increased temperature, which would reduce melt viscosity further and also melt PP quickly, caused an adverse effect, and the excessive swelling effect was observed again. The reduction of fibre volume fraction by adding neat PE pellets was also replicated by adding neat PP instead, which produced excessive swelling at both 170 and 190 T1 temperature settings.

For these reasons, it is believed something interesting is happening at the process temperature between the melting temperatures of PE and PP, as intended. The working theory is illustrated in Figure 5.7.

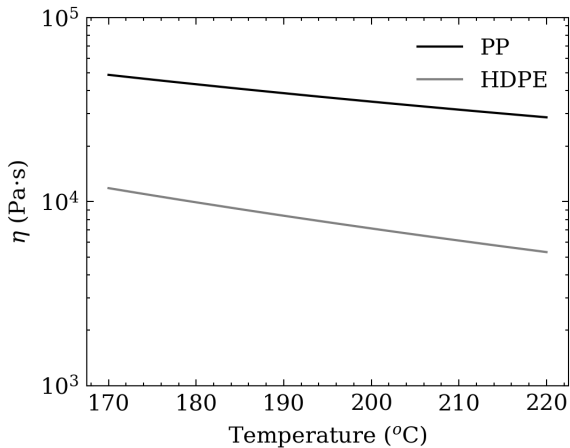


**Figure 5.5:** Shear viscosity at 1/s shear rate of HDPE and PP, adapted from [56, 57]

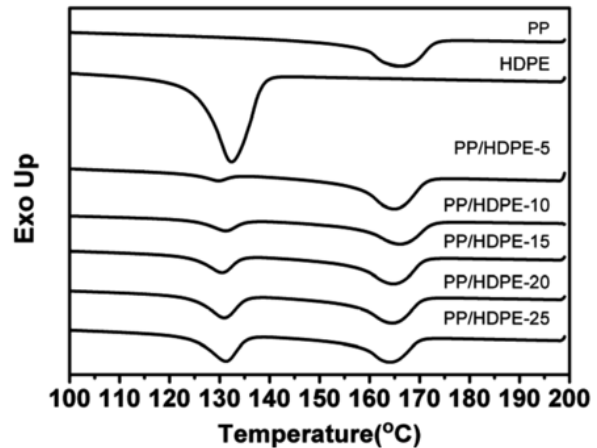


**Figure 5.6:** Melting peaks characterised by differential scanning calorimetry (DSC) of PP, HDPE and their blends [58]

### Delaying fibre release

As shown in Figure 5.6, PE has a lower melting temperature than the PP in the LGFPP pellets. PE melts first, which has two effects on heating PP pellets. First, the PE melting absorbs heat as it changes phase, then the low viscosity of PE melt acts as a lubricant for solid PP pellets.

Lowering friction is potentially significant as the heater bands regulating the temperature of the barrel are only partially responsible for the heating and melting of pellets. Mechanical energy from the screw causing friction from shearing and compression of pellets is typically responsible for 60-80% of the heating [52, 59]. The lubricating effect of PE could effectively keep the temperature lower in the first half of the screw extruder, which delays the melting of LF PP pellets and delays fibre release. As discussed in section 4.4, this shortens the residence time of loose fibres, reducing the degree of fibre entangling, which is believed to be the cause of the swelling.

### Effects on shear flow

In addition to delaying the melting of LGFPP pellets, HDPE could also allow the pellets to pre-align by macro shear-alignment before melting, reducing the degree of entangling by organising the fibres (in bulk pellet form) before they are allowed to interact. Even as the resins pass the material temperature zone and PP begins to melt, HDPE has two effects: polymer interface slip and wall slip. Both of which further help prevent fibre entanglement.

HDPE is known for increasing the wall slip speed in capillary flows [60, 61]. By increasing the wall slip speed, the difference in flow velocity between the wall and centre is lowered, reducing the shear rate gradient as shown in Figure 5.8 for both capillary flow (which is typical of the flow in the nozzle) and Couette flow (which is typical for the shearing between extruder barrel and screw shaft). In both cases, it can be seen that increasing the wall-slip speed reduces the gradient of the shear flow. Also, the maximum peak velocity would be reduced for the same flow rate, which further reduces this gradient. If the shear gradient is responsible for long fibre entanglement,

as discussed in section 4.3, decreasing the shear gradient by wall slip could be effective in decreasing entanglement at both the screw extruder and the nozzle.

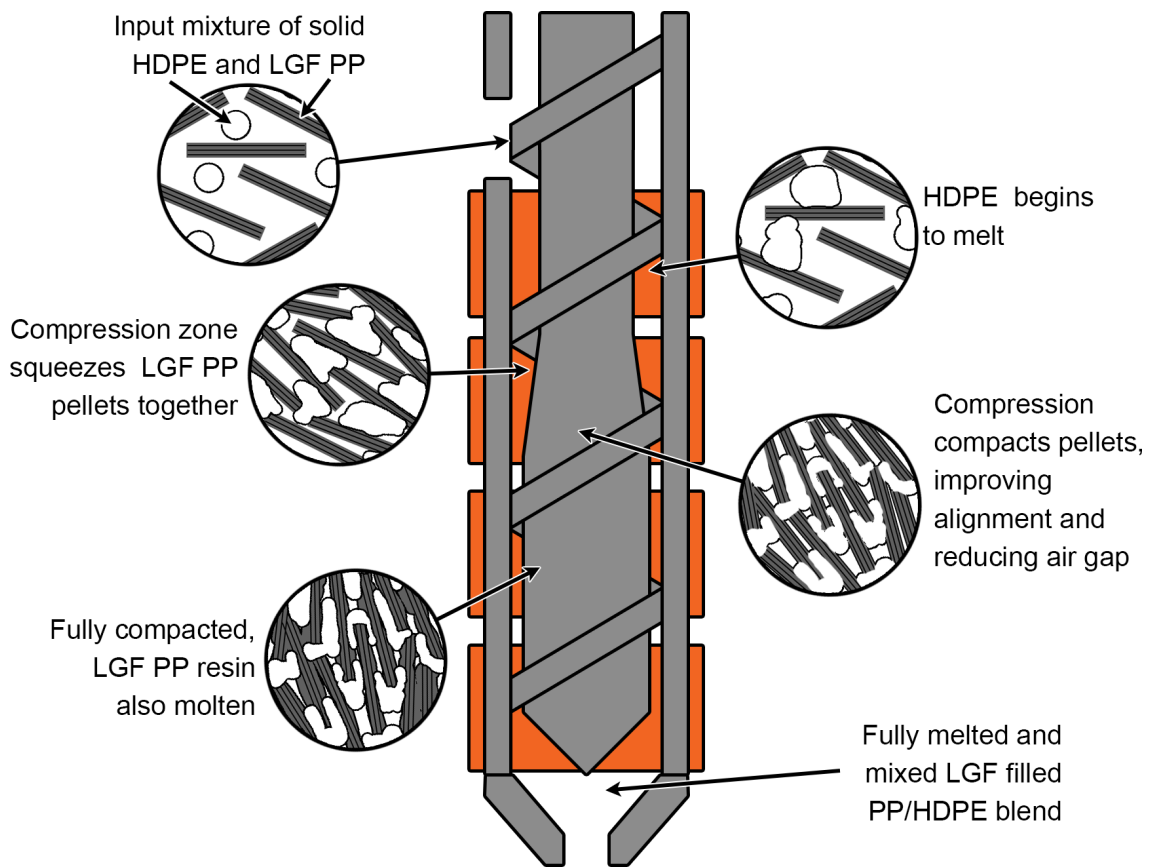
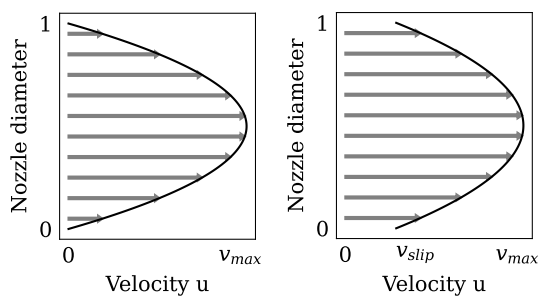


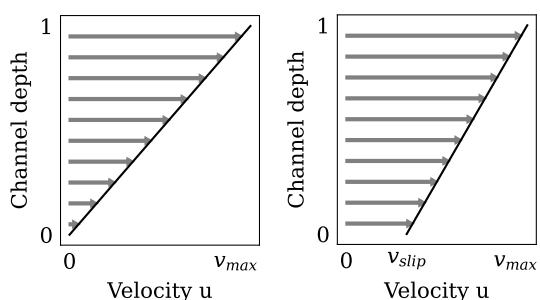
**Figure 5.7:** Hetero-phasic pellet transition along the screw extruder, HDPE melts first, allowing LGFPP to stay solid for longer. By allowing solid LGFPP to pre-compact and align before fibres are released by the resin, fibre entanglement is minimised

Slip also occurs at the interface between heterogeneous polymer melts of different viscosity [62, 63, 64]. HDPE and PP have different viscosity, as shown in Figure 5.5 (it should also be noted that fillers increase the viscosity [6, 65] of suspensions and the PP resin is filled with glass-fibres), and therefore, a discontinuous viscosity region exists between them. This is illustrated by Figure 5.9. This phenomenon causes PP and HDPE to slide against each other, mixing less together. This is believed to have two effects, it keeps the long fibres in LGFPP together for longer even after the PP resin is heated above its melting temperature as less mixing occurs.

Figure 5.10 and Figure 5.11 show cross-sections of LGFPP/PE blend sample, which shows discrete HDPE and fibre-rich regions, respectively. These are caused by the reduction in mixing from delaying fibre melting and the rheological effects HDPE has on the blend. While the lack of dispersion may have negative implications for the strength and consistency of the material, it is unavoidable with the currently developed strategy. It is preferable to under-mix fibres and resin rather than mix them too well, resulting in fibre die-swell and even lower strength.



(a) Zero wall-slip condition, capillary flow (b) Wall-slip condition, capillary flow



(c) Zero wall-slip condition, Couette flow (d) Wall-slip condition, Couette flow

Figure 5.8: Effect of wall slip on the shear flow field

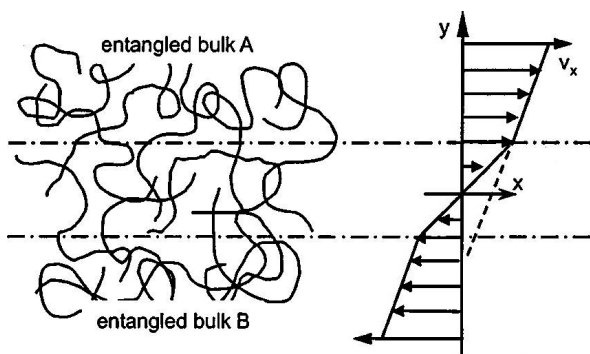


Figure 5.9: Fewer entangling polymer chains at the interface between two polymers of different viscosity causes a region of lower viscosity [62]



Figure 5.10: Sectioned microscopy of LGFPP/PE blend, showing a white region of discrete unmixed HDPE inside darker PP

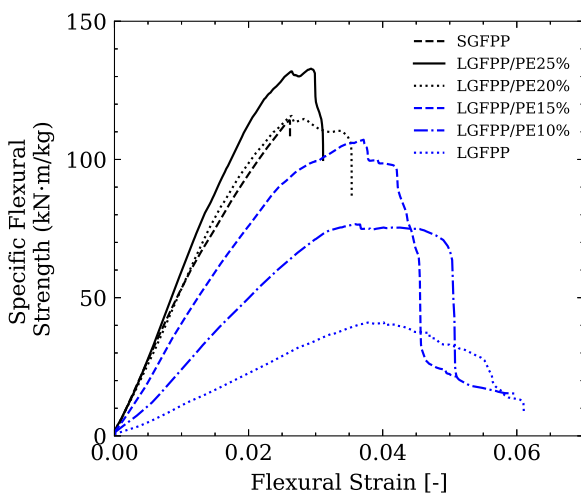


Figure 5.11: Sectioned microscopy of LGFPP/PE blend, showing un-dispersed fibre agglomerates

### 5.3. Mechanical Performance

The stress-strain curves of the free-extrusion three-point-bending tests are given in Figure 5.12, shown as specific strength after adjusting for density. Each material series is grouped by colour and one representative curve is highlighted for each series. The average mechanical properties of each sample series are given in Table 5.17. The LGFPP/PE blends vastly improve the neat LGFPP samples in strength and stiffness, with both properties increasing with increasing PE additive content. Notably, the 20 and 25% modified samples have higher specific properties than the short glass-fibre PP compound samples.

As expected, there is an increase in properties with decreased porosity in samples, this is shown in Figure 5.13. The addition of PE lowers the density of the resin as PE has a lower density than PP but the effect of decreasing porosity is dominant and density increases with higher PE content, shown in Table 5.16. It also shows that the addition of HDPE also dilutes the fibre content of the LFT PP pellets.



**Figure 5.12:** Representative stress-strain curves from three-point bending

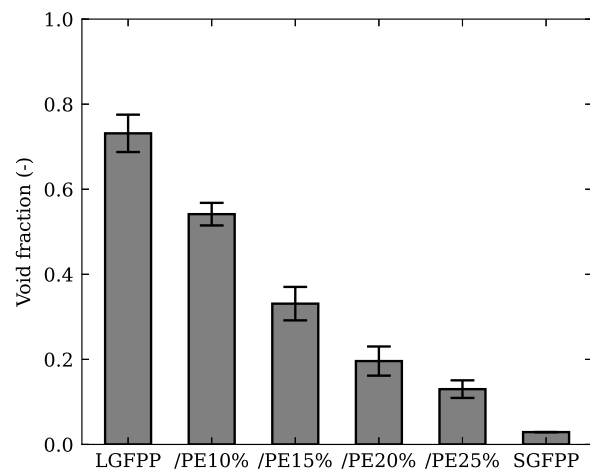


**Figure 5.13:** Average porosity (with 95% confidence interval)

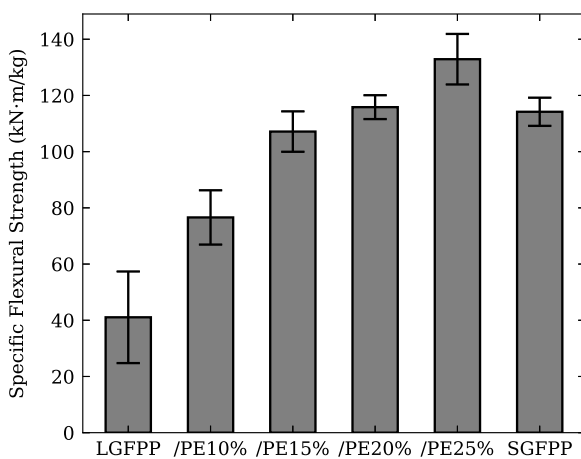


**Figure 5.14:** Average specific flexural strength (with 95% confidence interval)

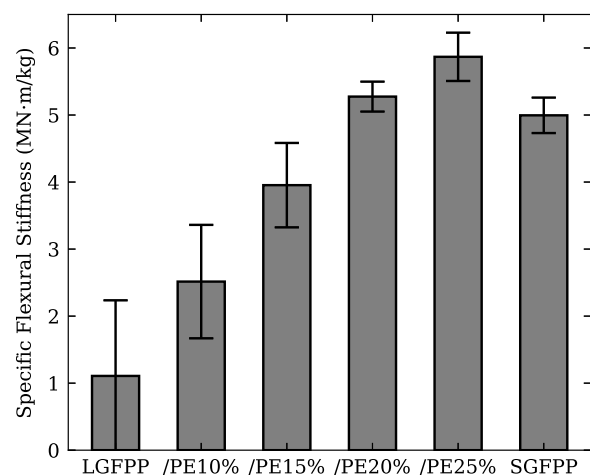


**Figure 5.15:** Average specific flexural stiffness (with 95% confidence interval)

Sample	Fibre Content (W/W%)	Density (g/cm <sup>3</sup> )	Sample count <i>n</i>
SGFPP	30	1.12	18
LGFPF	30	0.30	7
"/PE10%	28	0.51	16
"/PE15%	27	0.76	9
"/PE20%	26	0.90	7
"/PE25%	25	0.95	7

**Table 5.16:** Sample fibre content, average density, sample count used for mechanical testing

Sample	Flexural Strength (MPa)	Flexural Stiffness (GPa)	Specific Flexural Strength (kN·m/kg)	Specific Flexural Stiffness (MN·m/kg)
SGFPP	127.9	5.68	114.2	5.07
LGFPF	13.1	0.36	43.6	1.18
"/PE10%	41.4	1.35	82.0	2.67
"/PE15%	67.8	2.54	90.3	3.34
"/PE20%	96.4	4.26	113.8	4.72
"/PE25%	126.3	5.66	132.9	5.96

**Table 5.17:** Average strength, stiffness, calculated specific strength and stiffness values from mechanical testing

## 5.4. Microstructure Characterisation

### 5.4.1. Fibre length

The fibre length distribution (FLD) of the SGFPP, original LGFPF and modified LGFPF/PE extrudates were measured and are given in Figure 5.19. The modal fibre length of all LFT extrusions was under 1 mm. This fibre length attrition is due to fibres being mechanically loaded while their pellet is partially melted and as fibres make contact with each other and screw and barrel walls during mixing. Fibre attrition does not seem to be worse with the HDPE addition and low material transport temperature technique. There is a risk that the lower T1 transport temperature could cause excessive fibre attrition due to higher viscosity and rubbing of partially melted pellets, but this does not seem to be the case.

While the majority of fibres have been shortened by attrition (as expected from literature values), both the number average and weight average of fibres are significantly increased from the SFT fibre length shown in Figure 5.19a. ~70% of fibres exceed 1 mm in length and the weight average fibre length is close to the 2.6 mm critical fibre length from literature [9]. These long fibres are responsible for higher mechanical properties than the SGFPP.

	$\eta_l$
SGFPP	0.070
LGFPF	0.392
LGFPF/PE15%	0.392
LGFPF/PE25%	0.394

**Table 5.18:** Fibre length efficiency factor

The fibre length loading efficiency factors  $\eta_l$  of these measured lengths calculated according to Equation 1.3 are collected in Table 5.18 and also shown in each FLD. It shows the LGFPP extrudates have the potential to be 5x stronger than the SGFPP, barring differences in fibre orientation.

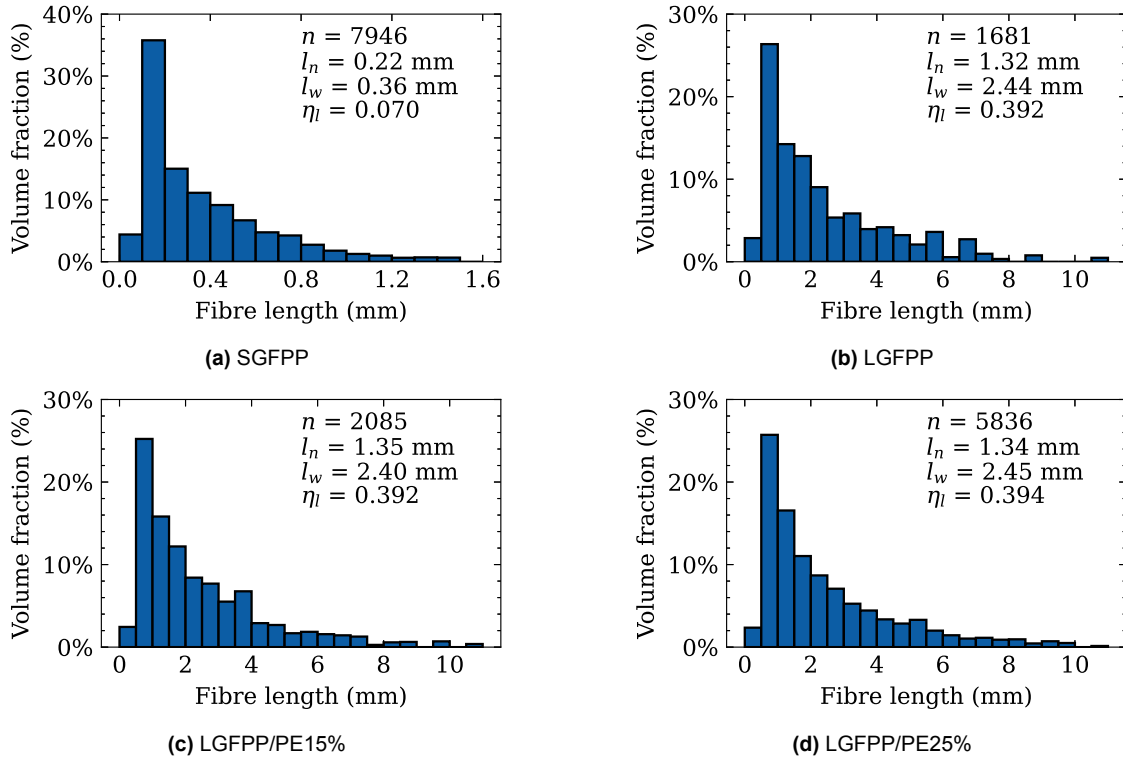


Figure 5.19: Fibre length distribution histograms

### 5.4.2. Fibre orientation

The FOD of the respective extrusions are shown in Figure 5.21, which show a slight improvement in alignment in all PE-modified samples over the unmodified LFT. Figure 5.21a shows the FOD of SGFPP, which shows moderate misalignment with an average fibre misalignment of  $18.3^\circ$ . In contrast, FOD analysis of LFT extrusions shows fibre misalignment is significantly higher at  $45\text{--}50^\circ$  from flow direction, with few to no fibres well aligned.

This is due to rotational memory, swirling of the material and fibres, caused by the reciprocal mixing of the screw extruder, which is retained even post-extrusion. Figure 5.22 shows groups of under-dispersed fibres distributed in swirls centred around the centre of the extrusion. It also shows a central cavity which was present in almost all LGFPP/PE extrusions. This central pore is caused by the swirling effect, causing expansion and tearing of the resin at the centre.

It should be noted that these results are not representative of the fibre alignment of future parts printed with this material. The difference between free-extrusion and ex-

	$\eta_o$
SGFPP	0.786
LGFPP	0.195
LGFPP/PE15%	0.159
LGFPP/PE25%	0.253

Table 5.20: Fibre orientation efficiency factor

trusion on previous layers is shown in Figure 3.9. Layer deposition on previous layers induces heavy shear and extensional alignment as the nozzle moves along the part, which would improve alignment. Also, the extrusion is flattened into 1-2 mm depending on the print layer height, which removes one angular component of misalignment from the fibre vector and could possibly compress the central cavity away.

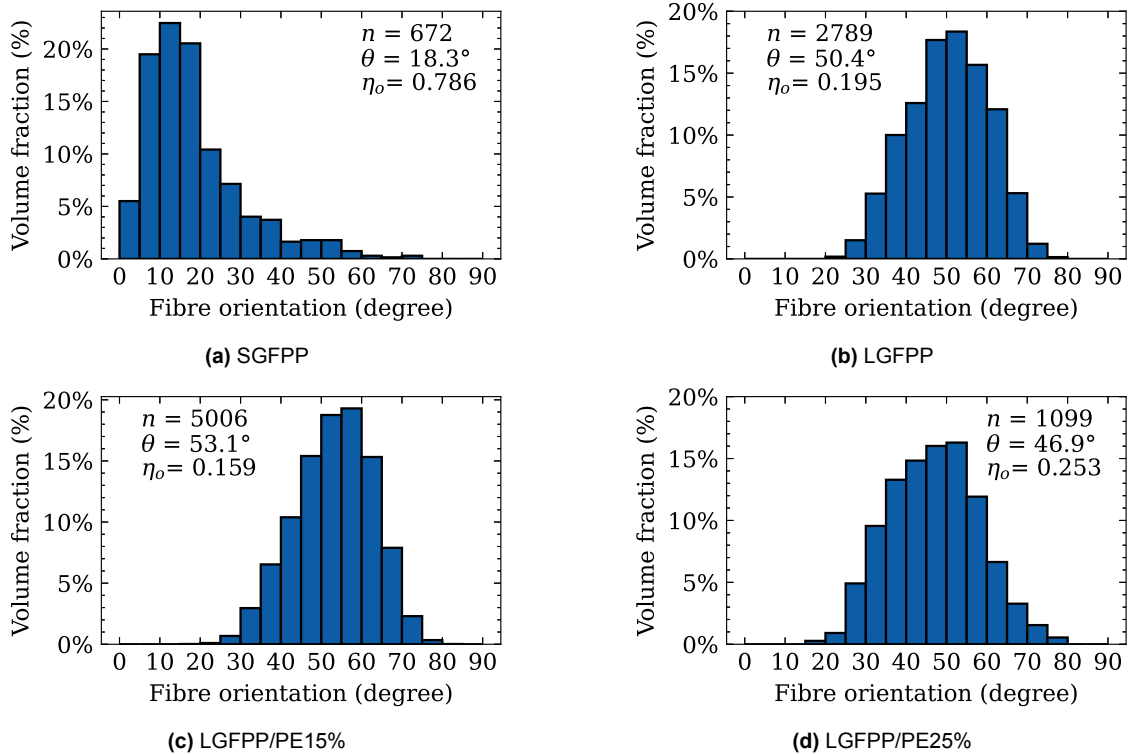
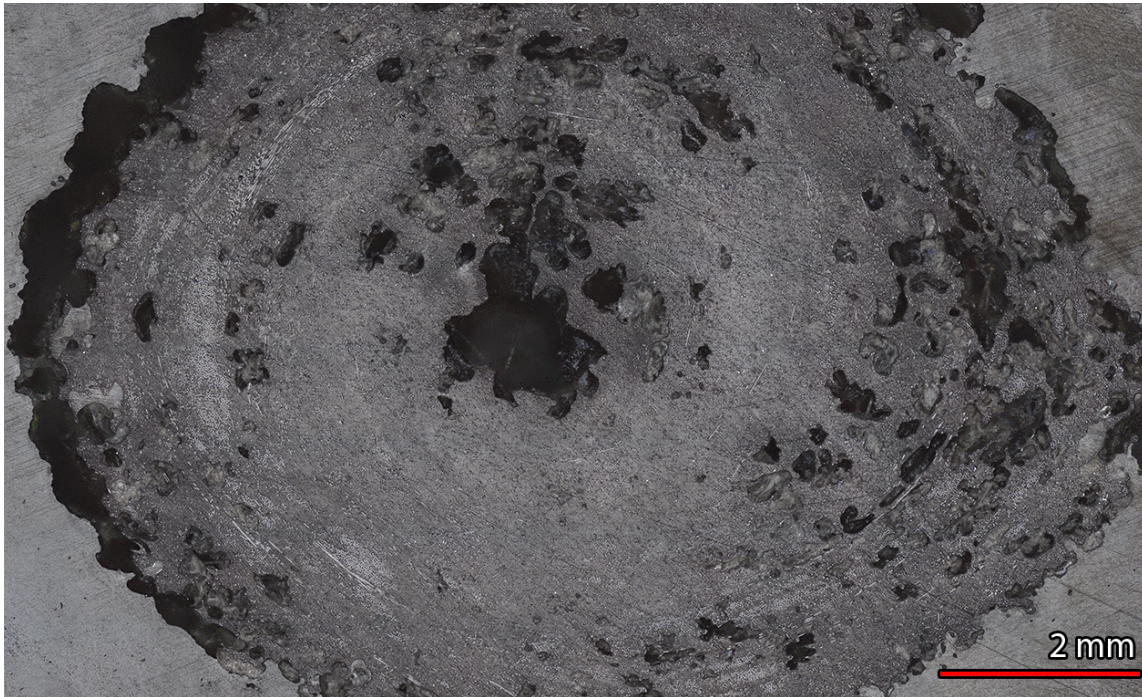


Figure 5.21: Fibre orientation distribution histograms

### 5.4.3. Summary of measured fibre efficiency factors

The fibre loading efficiency factor  $\eta_l$  and the fibre orientation factor  $\eta_o$  from section 5.4 and the fibre volume fraction  $V_f$  are combined together in Table 5.23 to give the first term of the rule of mixtures Equation 1.1  $\eta_l \eta_o V_f$ . Also given in Table 5.23 is the void volume fraction  $V_v$  and specific strengths from section 5.3.

It can be observed that while  $\eta_l$  is very good for the long-fibre compounds, almost six times that of SGFPP, the fibre orientation  $\eta_o$  leaves much to be desired. The misalignment causes the strength to be down-rated to a quarter of its potential. In all long fibre samples, the strength is impeded by high void content, despite having higher  $\eta_l \eta_o V_f$  values, porosity results in lower strength than SGFPP with the exception of LGFP-P/PE25%, which only achieves 16% higher specific strength despite having a  $\eta_l \eta_o V_f$  45% higher. It should also be noted that some of this weakness will be from the weaker PE blended resin, but this was not determined, so it was not further discussed.



**Figure 5.22:** Sectioned microscopy of 20% modified long fibre extrusion, showing large central pore

	$\eta_l$	$\eta_0$	$\eta_l\eta_0$	$V_f$	$\eta_l\eta_0V_f$	$V_v$	kN·m/kg
SGFPP	0.070	0.786	0.055	13.6%	0.0075	2.9%	114.2
LGFPF	0.392	0.195	0.077	13.6%	0.0104	73.1%	43.6
LGFPF/PE15%	0.392	0.159	0.062	11.8%	0.0074	33.1%	90.3
LGFPF/PE25%	0.394	0.253	0.100	10.9%	0.0109	13.0%	132.9

**Table 5.23:** Fibre efficacy terms  $\eta_l$ ,  $\eta_0$  and  $V_f$ , with  $V_v$  and specific flexural strength for reference

The  $\eta_l\eta_0V_f$  terms together represent the contribution of the fibres to the strength of the composite, based on its length, orientation and volume fraction. It can be seen that the long fibres of LGFPF/PE25% are more effective despite worse fibre orientation and lower fibre fraction than SGFPF due to its long fibre length. From the  $\eta_l\eta_0$  values, it can be seen that the utilisation of fibres is almost twice as high with LGFPF/PE25% over SGFPF.

# 6

## Conclusions & Recommendations

Large-scale 3D printing with long glass-fibre reinforced polypropylene pellets was explored to improve mechanical strength over short glass-fibre polypropylene, a standard printing material used in LSAM. It was hypothesised that longer reinforcing fibres could significantly improve strength by increasing fibre pullout stress.

However, an extreme die-swelling behaviour was found, which made the material unusable for 3D printing. Mechanical properties were very low due to extremely high ( $\sim 70\%$ ) porosity, and the swelling was high enough to make controlled material layup difficult. The cause of the swelling was identified as an entangled network of long fibres being compressed and storing energy during the convergent flow channel of the nozzle. Upon die-exit, these fibres release stress by expanding. The expansion is strong enough to fracture the molten matrix, creating voids.

The swelling was solved by adding polyethylene pellets with the long glass-fibre polypropylene. By using a temperature setting which delays the melting of polypropylene but melts polyethylene, fibre release from polypropylene is delayed. Also, HDPE has several special rheological slipping effects which reduce shear mixing. Together these reduce the degree of mixing and entanglement of fibres, eliminating swelling. This method significantly reduces the swelling, with the 25% HDPE blend reducing porosity by a factor of five and increasing strength ten-fold from the original swollen long glass-fibre polypropylene.

The modified long-fibre material achieves a specific strength and stiffness of 16% and 18% higher, respectively, over short glass-fibre polypropylene. These increased properties are achieved by having longer fibres. The modified long-fibre compound has a weight average fibre length of 2.5 mm, which is very close to the critical fibre length of 2.6 mm for glass-fibre in polypropylene. Though the fibre alignment efficiency factor is one-third of the much better aligned short-fibre compound, the fibre length loading factor is 5.6x as high due to the longer fibres. The fibre utility factor of the PE-modified long-fibre compound was almost twice as high as that of the short-fibre.

This thesis proves the concept of utilising long-fibre compounds to be extruded into beads with higher directional properties than the current standard short-fibre com-

pounds. Though the longer fibres almost doubled the fibre utilisation, its value was still only a tenth of an equivalent fibre fraction uni-directional, continuous composite. Even higher anisotropic properties could be achieved if porosity can be lowered and fibre alignment improved. Such a material shaped by the high shaping-freedom possible with additive manufacturing could create unprecedentedly strong and lightweight structures.

## 6.1. Recommendations

The processing technique developed in this thesis still has room for development. Although the achieved average fibre length of 2.5 mm is much higher than the 0.36 mm for the short-fibre compound, high anisotropic properties are obstructed by having relatively high porosity (13%) and an average measured fibre misalignment of 46°. Also, it is unclear to what degree fibre alignment would be improved and porosity eliminated after shearing against previous layers during 3D printing.

3D printing with this material has only been tested as a preliminary step, limited in scope to whether the reduction in swelling and stability of the material was sufficient for deposition. The optimal temperature settings, printing speed/layer time, and thermal stability were not examined yet and improved procedures could result in higher properties still due to shear alignment as the bead is laid down. It is hypothesised that the higher heat deflection temperature and entangled fibre network could result in a high rigidity of hot deposited layers, allowing for printing at higher speeds and with steeper overhangs. The possibility of printing at hotter speeds and fibre cross-linking between layers could also result in higher inter-layer adhesion strength.

Mechanical testing and material characterisation should be repeated after printing walls. This would have two benefits. Flat plates can be printed, which are more suitable for testing than round free-extruded samples. Also, the effect of shearing on fibre alignment, caused by shearing the extrudate against previous layers, can be studied.

The working mechanism of this method is not fully understood. Further testing and variation, especially of samples collected after cold-screw pullout, would help examine the fibre morphology and its interaction with HDPE. Cold-screw pullout was not possible because the hydraulic equipment necessary to pull the screw out was not available. Additionally, microscopy has limited ability to characterise the shape of fibres. Micro CT imaging of samples, especially cold-screw pullout samples, could offer crucial insight into fibre behaviour and void formation.

The addition of HDPE to LGFPP was done by simply mixing pellets. However, as they have different lengths, shapes and densities, this is not practical for large-scale industrial use. Stored pellets will separate over time, material transport may not be consistent, and there is less consistency in general during mixing and extrusion. The creation of a new type of pellet, for example, LGFPP co-extruded with a coating of HDPE, or dosing mechanisms which could more accurately mix the correct ratio of LGFPP and HDPE, should be explored.

This method was tested with LGFPP with 30% fibre weight fraction and HDPE. How-

ever, it would also be interesting to test this technique with other LFT materials and other low viscosity resins (such as low temperature modified PP) in lieu of HDPE to find superior material combinations with this technique. Unfortunately, mechanical testing only later revealed that even higher HDPE content could result in even stronger extrusions, further exploration in this direction could be interesting. As this technique minimises fibre interaction to make the material more processable, it would also be interesting to test if this holds for higher fibre loading materials for even higher directional properties.

Additionally, long-fibre printing could be explored as a way to recycle end-of-life composite parts, especially thermoplastic composite parts. Currently, recycling of composites is limited, often involving milling fibres to be used as short-fibre reinforcements. Long-fibre printing could offer a method of re-using composite fibres above the critical fibre length in length as feedstock, re-using the fibres at their maximum potential.

Finally, multi-axis slicing and printing should be developed and tested to take full advantage of highly anisotropic deposition beads once it has matured with improved properties. Long fibre printing also possibly offers the interesting ability to print high overhangs or free-form printing due to the higher melt strength of long fibre thermoplastics. Discontinuous fibre-reinforced additive manufacturing is mostly limited to so-called '2.5D printing', which limits deposition into parallel planar slices. However, complete freedom of bead placement, which has only been superficially developed at large-scale, would truly utilise the high anisotropic properties. Placing highly anisotropic beads aligned with the direction of stress fields could achieve even stronger and lighter parts, which is the dream of every structural engineer.



# References

- [1] ISO/ASTM. *52900 Additive manufacturing — General principles — Terminology*. Standard. 2015.
- [2] S. C. Joshi and A. A. Sheikh. “3D printing in aerospace and its long-term sustainability”. In: *Virtual and Physical Prototyping* 10.4 (2015), pp. 175–185. ISSN: 1745-2759 1745-2767. DOI: 10.1080/17452759.2015.1111519.
- [3] T. D. Ngo, A. Kashani, G. Imbalzano, K. T. Q. Nguyen, and D. Hui. “Additive manufacturing (3D printing): A review of materials, methods, applications and challenges”. In: *Composites Part B: Engineering* 143 (2018), pp. 172–196. ISSN: 13598368. DOI: 10.1016/j.compositesb.2018.02.012.
- [4] Sculpteo. *The State of 3D Printing 2021*. Pamphlet. 2021.
- [5] R. Gibson. *Principles of Composite Material Mechanics*. CRC Press, 2016. ISBN: 978 1 498 72072 4.
- [6] U. N. Gandhi, S. Goris, T. A. Osswald, and Y.-Y. Song. *Discontinuous Fiber-Reinforced Composites*. Hanser Publications, 2020. ISBN: 978-1-56990-694-1. DOI: 10.3139/9781569906958.
- [7] A. Kelly and W. R. Tyson. “Tensile properties of fibre-reinforced metals: Copper-tungsten and copper/molybdenum”. In: *Journal of the Mechanics and Physics of Solids* 13.6 (1965), pp. 329–350. ISSN: 00225096. DOI: 10.1016/0022-5096(65)90035-9.
- [8] J. L. Thomason and M. A. Vlуг. “Influence of fibre length and concentration on the properties of glass fibre-reinforced polypropylene: 1. Tensile and flexural modulus”. In: *Composites Part A: Applied Science and Manufacturing* 27.6 (1996), pp. 477–484. ISSN: 1359835X. DOI: 10.1016/1359-835x(95)00065-a.
- [9] J. L. Thomason, M. A. Vlуг, G. Schipper, and H. G. L. T. Krikor. “Influence of fibre length and concentration on the properties of glass fibre-reinforced polypropylene: Part 3. Strength and strain at failure”. In: *Composites Part A: Applied Science and Manufacturing* 27.11 (1996), pp. 1075–1084. ISSN: 1359835X. DOI: 10.1016/1359-835x(96)00066-8.
- [10] S. Krump. *Apparatus and method for creating three-dimensional objects*. Patent. 1989.
- [11] R. S. Gaur. “Buckling performance improvement in 3d printed variable stiffness composite laminates”. Thesis. 2022. DOI: <http://resolver.tudelft.nl/uuid:c00bc34d-47af-49fc-8119-714d49a9e100>.
- [12] W. Zhong, F. Li, Z. Zhang, L. Song, and Z. Li. “Short fiber reinforced composites for fused deposition modeling”. In: *Materials Science and Engineering: A* 301.2 (2001), pp. 125–130. ISSN: 09215093. DOI: 10.1016/s0921-5093(00)01810-4.

- [13] C. Duty et al. "What makes a material printable? A viscoelastic model for extrusion-based 3D printing of polymers". In: *Journal of Manufacturing Processes* 35 (2018), pp. 526–537. ISSN: 15266125. DOI: 10.1016/j.jmapro.2018.08.008.
- [14] L. G. Blok, M. L. Longana, H. Yu, and B. K. S. Woods. "An investigation into 3D printing of fibre reinforced thermoplastic composites". In: *Additive Manufacturing* 22 (2018), pp. 176–186. ISSN: 22148604. DOI: 10.1016/j.addma.2018.04.039.
- [15] S. Gantenbein, K. Masania, W. Woigk, J. P. W. Sesseg, T. A. Tervoort, and A. R. Studart. "Three-dimensional printing of hierarchical liquid-crystal-polymer structures". In: *Nature* 561.7722 (2018), pp. 226–230. ISSN: 1476-4687 (Electronic) 0028-0836 (Linking). DOI: 10.1038/s41586-018-0474-7.
- [16] K. Winter, J. Wilfert, B. Häupler, J. Erlmann, and V. Altstädt. "Large Scale 3D Printing: Influence of Fillers on Warp Deformation and on Mechanical Properties of Printed Polypropylene Components". In: *Macromolecular Materials and Engineering* 307.1 (2021). ISSN: 1438-7492 1439-2054. DOI: 10.1002/mame.202100528.
- [17] M. Borish et al. "In-Situ Thermal Imaging for Single Layer Build Time Alteration in Large-Scale Polymer Additive Manufacturing". In: *Procedia Manufacturing* 34 (2019), pp. 482–488. ISSN: 23519789. DOI: 10.1016/j.promfg.2019.06.202.
- [18] C. E. Duty et al. "Structure and mechanical behavior of Big Area Additive Manufacturing (BAAM) materials". In: *Rapid Prototyping Journal* 23.1 (2017), pp. 181–189. ISSN: 1355-2546. DOI: 10.1108/rpj-12-2015-0183.
- [19] H. Ning, N. Lu, A. A. Hassen, K. Chawla, M. Selim, and S. Pillay. "A review of Long fibre-reinforced thermoplastic or long fibre thermoplastic (LFT) composites". In: *International Materials Reviews* 65.3 (2019), pp. 164–188. ISSN: 0950-6608 1743-2804. DOI: 10.1080/09506608.2019.1585004.
- [20] Solvay. *Long Fiber Thermoplastics*. Web Page. 2021.
- [21] A. Inoue, K. Morita, T. Tanaka, Y. Arao, and Y. Sawada. "Effect of screw design on fiber breakage and dispersion in injection-molded long glass-fiber-reinforced polypropylene". In: *Journal of Composite Materials* 49.1 (2013), pp. 75–84. ISSN: 0021-9983 1530-793X. DOI: 10.1177/0021998313514872.
- [22] G. Tian, X. Liang, M. Wang, Y. Lei, G. Jin, and X. Wang. "Fiber breakage behavior of long glass fiber-reinforced polypropylene through the convergent channel". In: *Journal of Reinforced Plastics and Composites* 36.22 (2017), pp. 1629–1638. ISSN: 0731-6844 1530-7964. DOI: 10.1177/0731684417721977.
- [23] P. Ren and G. Dai. "Fiber dispersion and breakage in deep screw channel during processing of long fiber-reinforced polypropylene". In: *Fibers and Polymers* 15.7 (2014), pp. 1507–1516. ISSN: 1229-9197 1875-0052. DOI: 10.1007/s12221-014-1507-y.

- [24] J. Wang, C. Geng, F. Luo, Y. Liu, K. Wang, Q. Fu, and B. He. “Shear induced fiber orientation, fiber breakage and matrix molecular orientation in long glass fiber reinforced polypropylene composites”. In: *Materials Science and Engineering: A* 528.7-8 (2011), pp. 3169–3176. ISSN: 09215093. DOI: 10.1016/j.msea.2010.12.081.
- [25] C. Steger. “An unbiased detector of curvilinear structures”. In: *IEEE Transactions on Pattern Analysis and Machine Intelligence* 20.2 (1998), pp. 113–125. ISSN: 01628828. DOI: 10.1109/34.659930.
- [26] J. Schindelin et al. “Fiji: an open-source platform for biological-image analysis”. In: *Nat Methods* 9.7 (2012), pp. 676–82. ISSN: 1548-7105 (Electronic) 1548-7091 (Linking). DOI: 10.1038/nmeth.2019.
- [27] ASTM. *D2584 Standard Test Method for Ignition Loss of Cured Reinforced Resins*. Standard. 2021. DOI: 10.1520/d2584-18.
- [28] ASTM. *D3171 Standard Test Methods for Constituent Content of Composite Materials*. Standard. 2020. DOI: 10.1520/D3171-15.
- [29] U. W. Gedde and M. S. Hedenqvist. *Fundamental Polymer Science*. 2nd edition. Springer, 2019. ISBN: 978-3-030-29792-3. DOI: [https://doi.org/10.1007/978-3-030-29794-7\\_6](https://doi.org/10.1007/978-3-030-29794-7_6).
- [30] B. R. Byron, A. Robert C., and H. Ole. *Dynamics of Polymeric Liquids, Volume 1: Fluid Mechanics*. 1987. ISBN: 978-0-471-80245-7.
- [31] R. I. Tanner. “A theory of die-swell”. In: *Journal of Polymer Science Part A-2: Polymer Physics* 8.12 (1970), pp. 2067–2078. ISSN: 04492978 15429377. DOI: 10.1002/pol.1970.160081203.
- [32] S. Richardson. “The die swell phenomenon”. In: *Rheologica Acta* 9.2 (1970), pp. 193–199. ISSN: 0035-4511 1435-1528. DOI: 10.1007/bf01973479.
- [33] K. Wang. “Die Swell of Complex Polymeric Systems”. In: *Viscoelasticity - From Theory to Biological Applications*. 2012. Chap. Chapter 4. ISBN: 978-953-51-0841-2. DOI: 10.5772/50137.
- [34] W. W. Graessley, S. D. Glasscock, and R. L. Crawley. “Die Swell in Molten Polymers”. In: *Transactions of the Society of Rheology* 14.4 (1970), pp. 519–544. DOI: 10.1122/1.549177.
- [35] T. Nishimura and T. Kataoka. “Die swell of filled polymer melts”. In: *Rheologica Acta* 23.4 (1984), pp. 401–407. ISSN: 0035-4511 1435-1528. DOI: 10.1007/bf01329192.
- [36] A. M. Henderson and A. Rudin. “Effects of die temperature on extrudate swell in screw extrusion”. In: *Journal of Applied Polymer Science* 31.2 (1986), pp. 353–365. ISSN: 0021-8995. DOI: <https://doi.org/10.1002/app.1986.070310206>.
- [37] J. Z. Liang. “Effects of extrusion conditions on die-swell behavior of polypropylene/diatomite composite melts”. In: *Polymer Testing* 27.8 (2008), pp. 936–940. ISSN: 0142-9418. DOI: <https://doi.org/10.1016/j.polymertesting.2008.08.001>.

- [38] W.-Y. Chiu and G.-D. Shyu. "The study on die swell, fiber length distribution, and crystallinity of PP composite through extrusion". In: *Journal of Applied Polymer Science* 34.4 (1987), pp. 1493–1501. ISSN: 00218995 10974628. DOI: 10.1002/app.1987.070340413.
- [39] F. Henning, H. Ernst, and R. Brüssel. "LFTs for automotive applications". In: *Reinforced Plastics* 49.2 (2005), pp. 24–33. ISSN: 00343617. DOI: 10.1016/s0034-3617(05)00546-1.
- [40] EMS Grivory. *Long fibre reinforced polyamides Materials with spine*. Pamphlet. 2021.
- [41] A. Bechara, S. Goris, A. Yanev, D. Brands, and T. Osswald. "Novel modeling approach for fiber breakage during molding of long fiber-reinforced thermoplastics". In: *Physics of Fluids* 33.7 (2021), 1ENG. ISSN: 1070-6631 1089-7666. DOI: 10.1063/5.0058693.
- [42] D. M. Raymer and D. E. Smith. "Spontaneous knotting of an agitated string". In: *Proceedings of the National Academy of Sciences* 104.42 (2007), pp. 16432–16437. DOI: doi:10.1073/pnas.0611320104.
- [43] Y. Kim and O. O. Park. "Effect of Fiber Length on Mechanical Properties of Injection Molded Long-Fiber-Reinforced Thermoplastics". In: *Macromolecular Research* 28.5 (2020), pp. 433–444. ISSN: 1598-5032 2092-7673. DOI: 10.1007/s13233-020-8056-6.
- [44] E. Lafranche, P. Krawczak, J.-P. Ciolczyk, and J. Maugey. "Injection moulding of long glass fiber reinforced polyamide 66: Processing conditions/microstructure/flexural properties relationship". In: *Advances in Polymer Technology* 24.2 (2005), pp. 114–131. ISSN: 0730-6679 1098-2329. DOI: 10.1002/adv.20035.
- [45] T. T. Ngo, H. M. K. Nguyen, and D.-W. Oh. "Prediction of fiber rotation in an orifice channel during injection molding process". In: *Journal of Rheology* 65.6 (2021), pp. 1361–1371. ISSN: 0148-6055 1520-8516. DOI: 10.1122/8.0000314.
- [46] G. B. Jeffery and L. N. G. Filon. "The motion of ellipsoidal particles immersed in a viscous fluid". In: *Proceedings of the Royal Society of London. Series A, Containing Papers of a Mathematical and Physical Character* 102.715 (1997), pp. 161–179. ISSN: 0950-1207 2053-9150. DOI: 10.1098/rspa.1922.0078.
- [47] J. T. Hofmann, G. M. Vélez-García, D. G. Baird, and A. R. Whittington. "Application and evaluation of the method of ellipses for measuring the orientation of long, semi-flexible fibers". In: *Polymer Composites* 34.3 (2013), pp. 390–398. ISSN: 02728397. DOI: 10.1002/pc.22417.
- [48] L. H. Switzer and D. J. Klingenberg. "Rheology of sheared flexible fiber suspensions via fiber-level simulations". In: *Journal of Rheology* 47.3 (2003), pp. 759–778. ISSN: 0148-6055 1520-8516. DOI: 10.1122/1.1566034.
- [49] A. Salinas and J. F. T. Pittman. "Bending and breaking fibers in sheared suspensions". In: *Polymer Engineering and Science* 21.1 (1981), pp. 23–31. ISSN: 0032-3888 1548-2634. DOI: 10.1002/pen.760210105.

- [50] S. IPatcharaphun and G. Opaskornkul. *Characterization of Fiber Length Distribution in Short and Long-Glass-Fiber Reinforced Polypropylene during Injection Molding Process*. Conference Paper. 2008.
- [51] B. Franzén, C. Klason, J. Kubát, and T. Kitano. “Fibre degradation during processing of short fibre reinforced thermoplastics”. In: *Composites* 20.1 (1989), pp. 65–76. ISSN: 00104361. DOI: 10.1016/0010-4361(89)90684-8.
- [52] A. Altinkaynak, M. Gupta, M. A. Spalding, and S. L. Crabtree. “Melting in a Single Screw Extruder: Experiments and 3D Finite Element Simulations”. In: *International Polymer Processing* 26.2 (2011), pp. 182–196. ISSN: 2195-8602 0930-777X. DOI: 10.3139/217.2419.
- [53] S. A. Ahmad Ramazani, M. Abdi Valami, and M. Khak. “Effect of Poly (Propylene-g-maleic Anhydride) on the Morphological, Rheological, and Mechanical Properties of PP/HDPE Blend”. In: *Journal of Thermoplastic Composite Materials* 22.5 (2009), pp. 519–530. ISSN: 0892-7057 1530-7980. DOI: 10.1177/0892705709100662.
- [54] Y. Fujii, R. Nishikawa, P. Phulkard, and M. Yamaguchi. “Modifying the rheological properties of polypropylene under elongational flow by adding polyethylene”. In: *Journal of Rheology* 63.1 (2019), pp. 11–18. ISSN: 0148-6055 1520-8516. DOI: 10.1122/1.5049378.
- [55] M. Fujiyama and Y. Kawasaki. “Rheological properties of polypropylene/high-density polyethylene blend melts. I. Capillary flow properties”. In: *Journal of Applied Polymer Science* 42.2 (1991), pp. 467–480. ISSN: 00218995 10974628. DOI: 10.1002/app.1991.070420219.
- [56] E. Mitsoulis, H.-J. Luger, J. Miethlinger, and W. Friesenbichler. In: *International Polymer Processing* 33.5 (2018), pp. 642–651. DOI: doi:10.3139/217.3581. URL: <https://doi.org/10.3139/217.3581>.
- [57] F. Caffy and R. Nicolay. “Transformation of polyethylene into a vitrimer by nitroxide radical coupling of a bis-dioxaborolane”. In: *Polym. Chem.* 10 (23 2019), pp. 3107–3115. DOI: 10.1039/C9PY00253G. URL: <http://dx.doi.org/10.1039/C9PY00253G>.
- [58] J.-H. Lin et al. “Preparation and Compatibility Evaluation of Polypropylene/High Density Polyethylene Polyblends”. In: *Materials* 8.12 (2015), pp. 8850–8859. ISSN: 1996-1944. DOI: 10.3390/ma8125496.
- [59] Dynisco. *The Screw and Barrel System*. Pamphlet. 2021.
- [60] S. G. Hatzikiriakos and J. M. Dealy. “Wall slip of molten high density polyethylenes. II. Capillary rheometer studies”. In: *Journal of Rheology* 36.4 (1992), pp. 703–741. DOI: 10.1122/1.550313.
- [61] M. Ansari, S. G. Hatzikiriakos, and E. Mitsoulis. “Slip effects in HDPE flows”. In: *Journal of Non-Newtonian Fluid Mechanics* 167-168 (2012), pp. 18–29. ISSN: 0377-0257. DOI: <https://doi.org/10.1016/j.jnnfm.2011.09.007>.
- [62] R. Zhao and C. W. Macosko. “Slip at polymer–polymer interfaces: Rheological measurements on coextruded multilayers”. In: *Journal of Rheology* 46.1 (2002), pp. 145–167. DOI: 10.1122/1.1427912.

- [63] H. Furukawa. “Sliding along the interface of strongly segregated polymer melts”. In: *Physical Review A* 40.11 (1989), pp. 6403–6406. DOI: 10.1103/PhysRevA.40.6403.
- [64] P.-G. de Gennes. “Soft Matter (Nobel Lecture)”. In: *Angewandte Chemie International Edition in English* 31.7 (1992), pp. 842–845. ISSN: 0570-0833. DOI: <https://doi.org/10.1002/anie.199208421>.
- [65] A. Einstein. “Eine neue Bestimmung der Moleküldimensionen”. In: *Annalen der Physik* 324.2 (1906), pp. 289–306. ISSN: 00033804 15213889. DOI: 10.1002/andp.19063240204.



